



โครงการ การเรียนการสอนเพื่อเสริมประสบการณ์

ชื่อโครงการ จำลองโครงสร้างแถบพลังงานของระบบกราฟีนสองแผ่นที่ทำมุมบิดต่อกันโดยใช้
แบบจำลองการยึดเหนี่ยวแบบเหนียวแน่นของอิเล็กตรอน
Simulation of the electronic band structure of twisted bilayer graphene
using the tight-binding model

ชื่อนิสิต นายสุรยุทธ ปินตาวงศ์

เลขประจำตัว 5933449923

ภาควิชา ฟิสิกส์

ปีการศึกษา 2562

คณะวิทยาศาสตร์ จุฬาลงกรณ์มหาวิทยาลัย

Senior project
Simulation of the electronic band
structure of twisted bilayer graphene
using the tight-binding model

by

Surayuth Pintawong

Department of Physics
Chulalongkorn University

Dr. Thiti Taychatanapat
Advisor

Academic Year 2019

Contents

Abstract	3
Acknowledgement	4
1 Introduction	5
2 Theory	6
2.1 Untwisted graphene	6
2.1.1 Crystal structure of monolayer graphene	6
2.1.2 Tight binding model	6
2.1.3 Bilayer graphene	13
2.2 Twisted bilayer graphene	16
2.2.1 Crystal structure of twisted bilayer graphene	16
2.2.2 Continuum model of twisted bilayer graphene	21
2.2.3 Low energy regime of twisted bilayer graphene	23
3 Methodology	35
3.1 Large twist angles	35
3.2 Small twist angles	35
4 Result	36
4.1 Band structure along high symmetry lines and Bandwidth	36
4.2 three-dimensional band structures and Fermi surface	39
4.3 Density of states	41
5 Conclusion	43
Appendix	44
Appendix A	44
Appendix B	47
Appendix C	50

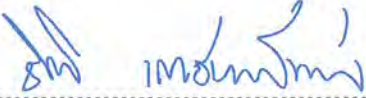
Project title Simulation of the electronic band structure of twisted bilayer graphene using the tight-binding model
Name Mr. Surayuth Pintawong
Department Physics
Academic year 2019
Project advisor Asst.Prof.Dr. Thiti Taychatanapat

accepted by the Department of Physics, Faculty of Science, Chulalongkorn University, in fulfillment for the degree of Bachelor of Science.

Project committees


..... Chairman
(Assoc.Prof.Dr. Udomsilp Pinsook)


..... Committee
(Dr. Annop Ektarawong)


..... Advisor
(Asst.Prof.Dr. Thiti Taychatanapat)

Project title	Simulation of the electronic band structure of twisted bilayer graphene using the tight-binding model
Name	Mr. Surayuth Pintawong
Department	Physics
Academic year	2019
Project advisor	Asst. Prof. Dr. Thiti Taychatanapat

Abstract

This senior project presents a model for calculating the band structure of twisted bilayer graphene for large and small twist angles using the tight-binding model. We also provide the program used for the calculations written on MATLAB 2018b. For large twist angles, we follow the model of A. O. Sboychakov. For small twist angles, we follow the model of A. H. MacDonald. We found that the magic angle, which yields minimum bandwidth, is equal to 1.05 degree which is agree with MacDonald's model and the density of states of twisted bilayer graphene at the magic angle is very high near the Fermi energy which suggests that the superconducting state can be obtained with the right conditions. Our model also shows that there are energy gaps on both sides of Fermi energy which means the insulating state of twisted bilayer graphene may be obtainable.

Keywords: twisted bilayer graphene, tight-binding model, magic angle

Acknowledgement

I would like to thank Asst.Prof.Dr.Thiti Taychatanapat for giving me advices, sparing his time for me and being very active. I also would like to thank Assoc.Prof.Dr. Udomsilp Pinsook and Dr. Annop Ektarawong for reviewing and criticizing my work.

Chapter 1

Introduction

Graphene is a two-dimensional layer of carbon atoms arranged on a honeycomb structure. Though the structure of graphite is a result of stacking of graphene, its electronic properties are different from graphene. For example, graphite can not conduct electricity and heat well, while graphene can conduct them very well. Because graphene is very thin, around 0.34 nm, it has a high potential to be used in electronics sectors. These exciting properties of graphene were first predicted theoretically by P. R. Wallace who wrote the first paper on the band structure of graphene in 1946[1]. Though graphene was discovered in 1962 by Hanns-Peter Boehm and his co-workers who coined the term graphene as combination graphite, it was hard to study and test properties of graphene because we didn't know how to produce graphene at that time. It is the work of a research group at the University of Manchester in 2004, led by Andre Geim and Konstantin Novoselov awarded with the Nobel Prize in Physics in 2010, who exfoliated graphene from bulk graphite by using sticky tape[2]. Graphene is an excellent conductor because the dispersion relation of electrons near the Fermi energy is linear[3]. We can also show that there is a possibility that an electron in graphene will tunnel perfectly through a potential barrier with no scattering[4, 5]. In the classical picture, this means particles can almost go straight through the graphene when we apply voltage to it, resulting in the high conductivity. In 2011, Allan MacDonald, a theoretical physicist at the University of Texas, Austin, and his colleagues predicted a flat band structure when we slightly twist two graphene sheet relative to each other[6]. Those twist angles which yield the flat bands are called magic angles. At magic angles, the densities of states are very high near the Fermi energy compared to other ranges of energy. There are also gaps forming above and below the flat bands. These imply that twisted bilayer graphene can be a superconductor and an insulator when we change its density of states. It was not until 2018 when Jarillo-Herrero and his team at MIT discovered that twisted bilayer graphene could be a superconductor and a Mott insulator when the twist angle is around 1.1° [7]. In this work, we want to simulate the band structure of twisted bilayer in two regimes, large and small twist angles. We will use the continuum model, which assumes the tunnelling amplitude between each π -orbitals to be an exponential function where the fitting parameters are obtained from graphene and untwisted bilayer graphene[8]. For large twist angles, the Hamiltonian is constructed according to the model of A. O. Sboychakov which calculates all possible tunnelling between carbon atoms in two layers[9]. Though we can get dispersion relations, with accuracy up to high energy, it's computationally expensive as the dimension of the Hamiltonian that we have to diagonalize is roughly proportional to $10^4\theta^{-2}$ (measured in degree) for low twisted angles. Thus, we will use this model only for the large twist angles, less than 30° . For the small twist angles, we use the model proposed by Allan MacDonald which calculates only the tunnelling between low-energy states. Though this model is valid for small twist angle $< 10^\circ$ and low-energy regime, the dimension of the Hamiltonian that we have to diagonalize in this case is proportional to $10\theta^{-2}$. We will do all the calculations on MATLAB.

Chapter 2

Theory

2.1 Untwisted graphene

2.1.1 Crystal structure of monolayer graphene

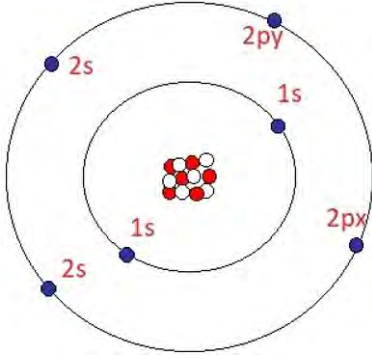


Figure 1: The valence electrons in the orbitals $2s, 2p_x$ and $2p_y$ forms the sp^2 orbitals leaving the last electron in the $2s$ orbital which will be in the $2p_z$ orbital later.

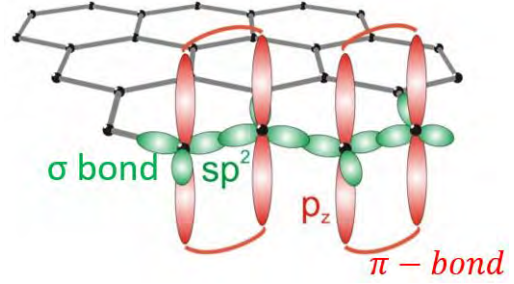


Figure 2: The bonds between the sp^2 orbitals, sigma bonds, are stronger than the bonds between $2p_z$ orbitals, pi bonds. Thus, each carbon atom has only one electron in the $2p_z$ orbitals that can move to nearby $2p_z$ orbitals.

The structure of graphene is a two-dimensional honeycomb of carbon atoms. Each carbon atom has six electrons where four of them are valence electrons. The valence electrons in $2s, 2p_x$ and $2p_y$ orbitals hybridize to form sp^2 orbitals, see Fig.1. The last electron in $2s$ orbital is promoted to the $2p_z$ orbitals. The bonds between the sp^2 orbitals, σ -bonds, are much stronger than the bonds between $2p_z$ orbitals, π -bonds, see Fig.2. This means electrons in the sp^2 orbitals can rarely go or interact with other orbitals while the electrons in $2p_z$ orbitals can. Thus, we will assume that each carbon atom has only one electron in its $2p_z$ orbital that can interact with a potential or tunnel to other sites. From Fig.4, We can choose primitive lattice vectors

$$\mathbf{a}_1 = a \left(\frac{\sqrt{3}}{2}, -\frac{1}{2} \right), \quad \mathbf{a}_2 = a \left(\frac{\sqrt{3}}{2}, \frac{1}{2} \right) \quad (1)$$

to describe the structure of graphene where $a = 2.46 \text{ \AA}$ is the distance between the lattice point. The distance between two adjacent carbon atoms are $a/\sqrt{3} \approx 1.46 \text{ \AA}$. There are two bases per lattice point in this case. The ones that are put directly on each lattice point are called A-sublattice, while the ones that are put relative to each lattice point are called B-sublattice. Thus, we can describe the points in the A-sublattice by a lattice vector $\mathbf{R}_A = n\mathbf{a}_1 + m\mathbf{a}_2$ and $\mathbf{R}_B = \mathbf{R}_A + \boldsymbol{\delta}_1$, see Fig.4, for the points in the B-sublattice. The unit cell of graphene is the region inside the dashed line.

2.1.2 Tight binding model

In this section, we will construct the Hamiltonian which is needed to be diagonalized later to obtain the band structure of twisted bilayer graphene. We will derive the Hamil-

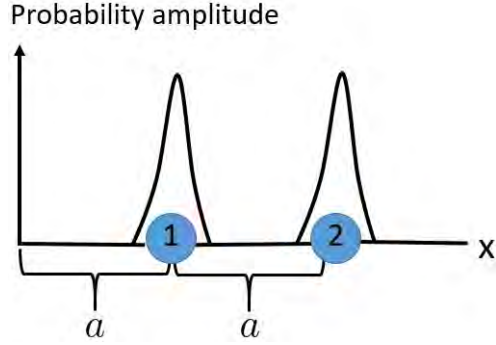


Figure 3: The distance between the atoms, which don't to be carbons, 1 and 2 is a . The wave functions of each electron are localized near each atom which means the probability amplitude is high in the region near each atom. Due to the localization of the wave function, there is almost no overlap region. This means the overlap integral almost vanishes.

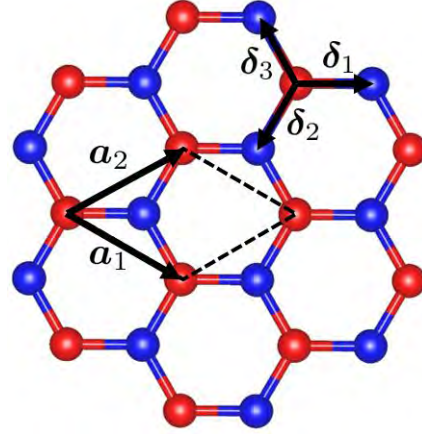


Figure 4: The structure of carbon atoms in a graphene sheet where the unit cell is the region in the black lines. The A(B) sub-lattices are colored as red(Blue), respectively. We choose $\mathbf{a}_1 = a(\sqrt{3}/2, -1/2)$ and $\mathbf{a}_2 = a(\sqrt{3}/2, 1/2)$ to be lattice vectors for both sub-lattice where the distance between AA(BB) sub-lattices, which will be used more regularly, is equal to $a = \sqrt{3}d = 2.46 \text{ \AA}$ where $d = 1.42 \text{ \AA}$ is the distance between carbon atoms. These vectors always point to the same sub-lattice sites and it's clear from the figure that each carbon atom has 3 neighbors.

tonian for graphene and bilayer graphene first and generalize the Hamiltonian to more complex systems later. To construct the Hamiltonian of an electron in graphene, first, we need to construct the wave function of an electron. We will use the tight-binding model which approximates the wave function of an electron to localize near each atom. Fig.3 illustrates the idea. By using this idea, we can approximate the wave function of an electron in graphene, which is a linear combination of the wave functions of electrons localized near each carbon atom, as

$$|\mathbf{k}\rangle = \sum_{\mathbf{r}_A} \phi_{\mathbf{r}_A, \mathbf{k}} |\mathbf{r}_A\rangle + \sum_{\mathbf{r}_B} \phi_{\mathbf{r}_B, \mathbf{k}} |\mathbf{r}_B\rangle \quad (2)$$

$$= c_A \sum_{\mathbf{r}_A} \frac{e^{i\mathbf{r}_A \cdot \mathbf{k}}}{\sqrt{N_{uc}}} |\mathbf{r}_A\rangle + c_B \sum_{\mathbf{r}_B} \frac{e^{i\mathbf{r}_B \cdot \mathbf{k}}}{\sqrt{N_{uc}}} |\mathbf{r}_B\rangle = c_A |A, \mathbf{k}\rangle + c_B |B, \mathbf{k}\rangle. \quad (3)$$

We use this trial wave function because the carbon atoms around sub-lattice A and B are different. Thus, the probability of finding an electron in each sub-lattice may be different. All the coefficients ϕ in Eq.2 represent the probability of finding an electron in each site of the carbon atoms. Thus, if the graphene sheet is huge, we expect the probability of finding an electron in the same sub-lattices to be equal even though the positions of the sites are different. From Eq.3, the probability of finding an electron in the A and B sub-lattices are $|c_A|^2$ and $|c_B|^2$, respectively. The factor $1/\sqrt{N_{uc}}$ is just a normalization factor and N_{uc} is equal to the number of unit cells in the graphene sheet. The reason for factoring out the exponential terms from each ϕ is because our wave function must satisfy Bloch's theorem (we are using periodic boundary condition here).

Now, the wave function can be written as a vector with two bases $|A\rangle$ and $|B\rangle$. To find the band structure, we start from the fact that the wave function of an electron must be an eigenvector of a Hamiltonian in order to find its energy. Thus, the wave function of an electron must satisfy the relation

$$H|\mathbf{k}\rangle = c_A H|A, \mathbf{k}\rangle + c_B H|B, \mathbf{k}\rangle = E_k |\Psi\rangle = E_k c_A |A, \mathbf{k}\rangle + E_k c_B |B, \mathbf{k}\rangle. \quad (4)$$

By acting $\langle A, \mathbf{k}|$ or $\langle B, \mathbf{k}|$ on the Eq.4 and rearranging the two equations, we get

$$\begin{bmatrix} \langle A, \mathbf{k}|H|A, \mathbf{k}\rangle & \langle A, \mathbf{k}|H|B, \mathbf{k}\rangle \\ \langle B, \mathbf{k}|H|A, \mathbf{k}\rangle & \langle B, \mathbf{k}|H|B, \mathbf{k}\rangle \end{bmatrix} \begin{bmatrix} c_A \\ c_B \end{bmatrix} = E_k \begin{bmatrix} \langle A, \mathbf{k}|A, \mathbf{k}\rangle & \langle A, \mathbf{k}|B, \mathbf{k}\rangle \\ \langle B, \mathbf{k}|A, \mathbf{k}\rangle & \langle B, \mathbf{k}|B, \mathbf{k}\rangle \end{bmatrix} \begin{bmatrix} c_A \\ c_B \end{bmatrix} \quad (5)$$

The first matrix on the left-hand side in Eq.5 is the Hamiltonian of our system. The first matrix on the right-hand side will vanish if the basis are orthogonal. The values of the diagonal terms of the matrix are 1. The values of the off-diagonal terms are

$$\langle A, \mathbf{k}|B, \mathbf{k}\rangle = \langle B, \mathbf{k}|A, \mathbf{k}\rangle^* = \sum_{\mathbf{r}_A} \sum_{\mathbf{r}_B} \frac{e^{i(\mathbf{r}_B - \mathbf{r}_A) \cdot \mathbf{k}}}{N_{uc}} \langle \mathbf{r}_A | \mathbf{r}_B \rangle. \quad (6)$$

For simplicity, the overlap integral $\langle \mathbf{r}_A | \mathbf{r}_B \rangle$ are vanished for our tight-binding model (Fig.3). The last step before diagonalizing the Hamiltonian is to specify the hopping integral $\langle \mathbf{r}_\alpha | H | \mathbf{r}_\beta \rangle$ where α and β can be A or B. From Fermi's golden rule, we can interpret this term as a quantity which tells us the probability of an electron to tunnel from a site \mathbf{r}_A to a site \mathbf{r}_B . Due to the tight-binding approximation, we only care about the tunnelling between nearest-neighbour electrons or

$$\langle \mathbf{r}_\alpha | H | \mathbf{r}_\beta \rangle = \begin{cases} \varepsilon, & \text{if } \mathbf{r}_\alpha = \mathbf{r}_\beta, \\ -t, & \text{if } |\mathbf{r}_\alpha - \mathbf{r}_\beta| = d, \\ 0, & \text{if } |\mathbf{r}_\alpha - \mathbf{r}_\beta| > d \end{cases} \quad (7)$$

where d is the distance between carbon atoms, Fig.4. Now, The upper-diagonal term of the Hamiltonian can be written as

$$\langle A, \mathbf{k}|H|A, \mathbf{k}\rangle = \sum_{\mathbf{r}_A} \sum_{\mathbf{r}_{A'}} \frac{e^{i(\mathbf{r}_{A'} - \mathbf{r}_A) \cdot \mathbf{k}}}{N_{uc}} \langle \mathbf{r}_A | H | \mathbf{r}_{A'} \rangle = \sum_{\mathbf{r}_A} \frac{\varepsilon}{N_{uc}} = \varepsilon. \quad (8)$$

The calculation in Eq.8 is simplified from the fact that an electron can only tunnel to its site or its nearest-neighbours. Thus, the non-vanishing terms must satisfy the condition $\mathbf{r}_A = \mathbf{r}_{A'}$. By doing the same calculation, we can get the values of $\langle B|H|B\rangle$. For the off-diagonal terms of the Hamiltonian, we can write to them as

$$\langle A, \mathbf{k}|H|B, \mathbf{k}\rangle = \langle B, \mathbf{k}|H|A, \mathbf{k}\rangle^* = \sum_{\mathbf{r}_A} \sum_{\mathbf{r}_B} \frac{e^{i(\mathbf{r}_B - \mathbf{r}_A) \cdot \mathbf{k}}}{N_{uc}} \langle \mathbf{r}_A | H | \mathbf{r}_B \rangle = \sum_{\mathbf{r}_A} -\frac{t}{N_{uc}} (e^{i\delta_1 \cdot \mathbf{k}} + e^{i\delta_2 \cdot \mathbf{k}} + e^{i\delta_3 \cdot \mathbf{k}}) \quad (9)$$

$$= -t(e^{i\delta_1 \cdot \mathbf{k}} + e^{i\delta_2 \cdot \mathbf{k}} + e^{i\delta_3 \cdot \mathbf{k}}). \quad (10)$$

To understand the calculation in Eq.9, we must realize that the non-vanishing terms from the first summation on \mathbf{r}_B are the terms that $\mathbf{r}_B = \mathbf{r}_A + \boldsymbol{\delta}_i$ where $i = 1, 2, 3$ (Fig.4). It's clear that, from Fig.4, $\boldsymbol{\delta}_1 = d(1, 0)$, $\boldsymbol{\delta}_2 = d(-1/2, -\sqrt{3}/2)$ and $\boldsymbol{\delta}_3 = d(-1/2, \sqrt{3}/2)$. Thus, there are only 3 non-vanishing terms for each \mathbf{r}_A , the nearest neighbors of each carbon atom in graphene are 3. If we define $f(\mathbf{k}) = e^{i\boldsymbol{\delta}_1 \cdot \mathbf{k}} + e^{i\boldsymbol{\delta}_2 \cdot \mathbf{k}} + e^{i\boldsymbol{\delta}_3 \cdot \mathbf{k}}$, the Hamiltonian can be fully written as

$$H = \begin{bmatrix} \varepsilon & -tf(\mathbf{k}) \\ -tf(\mathbf{k})^* & \varepsilon \end{bmatrix} = \begin{bmatrix} 0 & -tf(\mathbf{k}) \\ -tf(\mathbf{k})^* & 0 \end{bmatrix} + \varepsilon \begin{bmatrix} 1 & 0 \\ 0 & 1 \end{bmatrix}. \quad (11)$$

We can see that if we diagonalize effective Hamiltonian defined as $H^{eff} = H - \varepsilon \mathbf{1}$, the eigenvalues of H^{eff} are $\tilde{\lambda} = \lambda - \varepsilon$ where λ are the eigenvalues of H . Thus, the bands from H^{eff} are shifted by ε from the bands from H . However, they still capture the rest information of the real bands. So, for simplicity, we will set ε to 0. In other words, we will only work on the effective Hamiltonian later. Diagonalizing the Hamiltonian yields the eigenvalues

$$E_k = \pm t|f(\mathbf{k})| = \pm t \sqrt{1 + 4\cos^2\left(\frac{k_y a}{2}\right) + 4\cos\left(\frac{k_y a}{2}\right)\cos\left(\frac{k_x \sqrt{3}a}{2}\right)}. \quad (12)$$

The band structure E_k is shown in Fig.6. Fig.5 shows the first Brillouin zone of graphene spanned from two reciprocal lattice vectors.

$$\mathbf{b}_1 = \frac{2\pi}{a} \left(\frac{1}{\sqrt{3}}, -1 \right), \quad \mathbf{b}_2 = \frac{2\pi}{a} \left(\frac{1}{\sqrt{3}}, 1 \right). \quad (13)$$

As you can see, the shape of the first Brillouin zone is hexagonal and the points where the two bands contact are named as K or K' . This results from the fact that the forms of the low-energy effective Hamiltonian near the points K and K' are different which can be shown to be

$$H_{low}^{eff}(\mathbf{q}) = \begin{bmatrix} 0 & -tf(K+\mathbf{q}) \\ -tf(K+\mathbf{q})^* & 0 \end{bmatrix} \approx -t \begin{bmatrix} 0 & \nabla f'(K) \cdot \mathbf{q} \\ \nabla f'(K)^* \cdot \mathbf{q} & 0 \end{bmatrix} + O(|\mathbf{q}|^2). \quad (14)$$

From

$$f(\mathbf{k}) = e^{i\boldsymbol{\delta}_1 \cdot \mathbf{k}} + e^{i\boldsymbol{\delta}_2 \cdot \mathbf{k}} + e^{i\boldsymbol{\delta}_3 \cdot \mathbf{k}} = 2e^{ik_x a/(2\sqrt{3})} \cos\left(\frac{k_y a}{2}\right) + e^{-ik_x a/\sqrt{3}}, \quad (15)$$

It's straightforward to show that

$$\nabla f(\mathbf{k}) = e^{ik_y a/(2\sqrt{3})} \left(-a \sin\left(\frac{k_x a}{2}\right), \frac{a}{\sqrt{3}} \cos\left(\frac{k_x a}{2}\right) i - e^{-i\sqrt{3}k_y a/2} \frac{a}{\sqrt{3}} i \right). \quad (16)$$

Thus, if we use $K = (\mathbf{b}_2 - \mathbf{b}_1)/3 = (0, 4\pi/3a)$ (we can use other K points but the results will be the same), the low-energy effective Hamiltonian can be written as

$$H_{low,K}^{eff}(\mathbf{q}) = -t \begin{bmatrix} 0 & \sqrt{3}a/2(1, -i) \cdot \mathbf{q} \\ \sqrt{3}a/2(1, i) \cdot \mathbf{q} & 0 \end{bmatrix} = -\frac{\sqrt{3}ta}{2} \begin{bmatrix} 0 & q_x - q_y i \\ q_x + q_y i & 0 \end{bmatrix}. \quad (17)$$

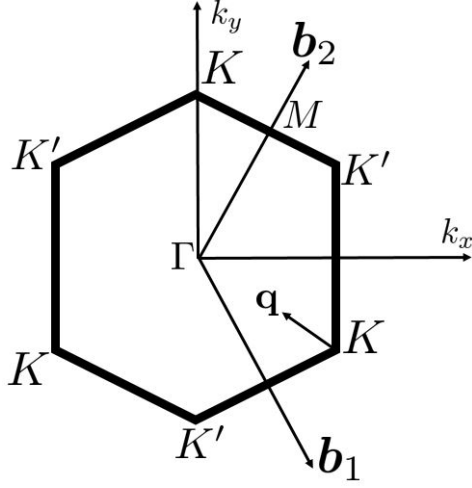


Figure 5: The first Brillouin zone of monolayer graphene is shown here. \mathbf{b}_1 and \mathbf{b}_2 are reciprocal lattice vectors and the vector \mathbf{q} is the vector measured from each Dirac point.

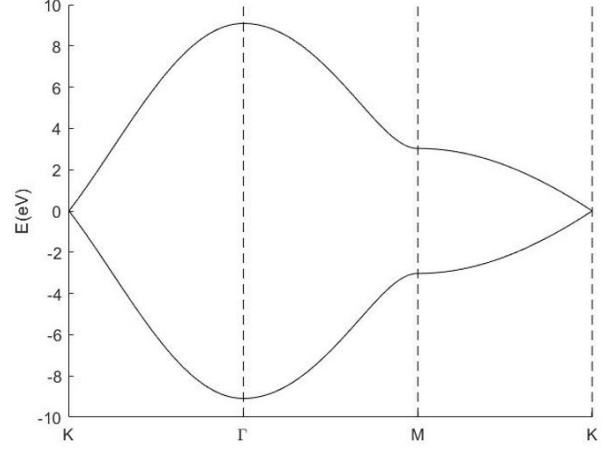


Figure 6: The band structure of monolayer graphene is shown here. The two bands arise from the fact that our wave function has two basis $|A\rangle, |B\rangle$. We plot the band structure along $K \rightarrow \Gamma \rightarrow M \rightarrow K$, see Fig.5. We use $t = 3.03\text{eV}$ and $a = 2.46 \text{ \AA}$ for these bands.

If we use $K' = -K$, from Eq.16,

$$H_{low,K}^{eff}(\mathbf{q}) = -t \begin{bmatrix} 0 & \sqrt{3}a/2(-1, -i) \cdot \mathbf{q} \\ \sqrt{3}a/2(-1, i) \cdot \mathbf{q} & 0 \end{bmatrix} = -\frac{\sqrt{3}ta}{2} \begin{bmatrix} 0 & q_x - q_y i \\ q_x + q_y i & 0 \end{bmatrix} \quad (18)$$

which has a different form from the low-energy effective Hamiltonian in Eq.17. This is the reason why those points are called differently. If we find the eigenvalue of the Hamiltonian near these points, it's equal to

$$E_k(\mathbf{q}) = \pm \frac{\sqrt{3}ta}{2} |\mathbf{q}| \quad (19)$$

which is a linear function of $|\mathbf{q}|$. Thus, the dispersion relation of electrons near K and K' is linear which is the reason why we call those points as "Dirac points". The Fermi velocity of electrons in graphene near the Dirac points is equal to

$$v_F = \frac{|\nabla_{\mathbf{k}} E_k(\mathbf{q})|}{\hbar} = \frac{\sqrt{3}ta}{2\hbar} \sim 10^6 \text{ m/s}. \quad (20)$$

Next, we will find the available states per band so that we can determine where the last electron is. The number of available states per band N_{as} can be written as

$$N_{as} = 2 \frac{A_{BZ}}{A_{state}} = \frac{4\sqrt{3}L_x L_y}{3a^2} = 2 \frac{A_{graphene}}{A_{uc}} = 2N_{uc} = N_{electron} \quad (21)$$

where A_{BZ} is the area of the first Brillouin zone and A_{state} is the area occupied by a state \mathbf{k} . The factor 2 arises from the fact that each \mathbf{k} -point can contain 2 electrons having spin up and down. In Eq.21, the area of the first Brillouin zone is $3\sqrt{3}/2(8\pi/(3a))^2$ and the area of each occupied state is equal to $\Delta k_x \Delta k_y = (2\pi/L_x)(2\pi/L_y)$ where L_x and

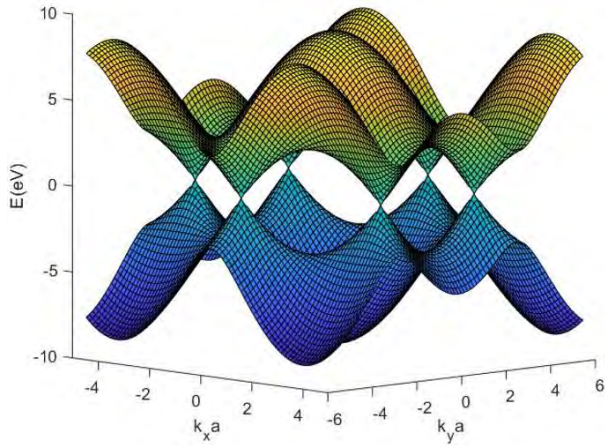


Figure 7: The valence and conduction bands.

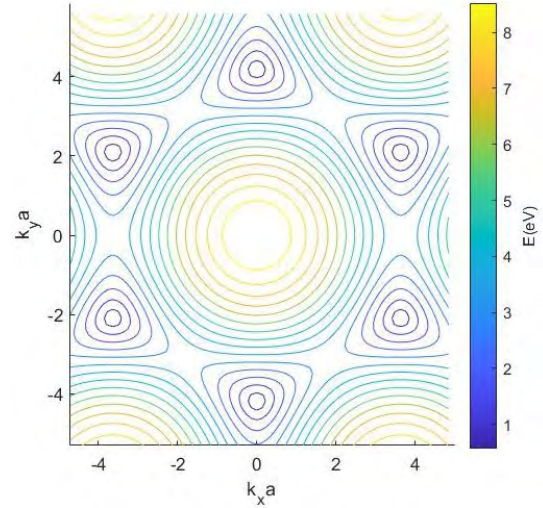


Figure 8: The Fermi surface of the conduction band.

L_x and L_y are the width and length of the graphene sheet. Note that quantized values of k_x and k_y comes from the fact that we're using the periodic boundary condition here. By inserting $L_x L_y$ to be the area of the graphene sheet and writing a^2 in terms of the area of each unit which is equal to $2A_{uc}/\sqrt{3}$, we can see that the number of the available states per band N_{as} is precisely equal to $2N_{uc}$, where N_{uc} is the number of unit cell in the graphene sheet. Because there are 2 electrons in the p_z orbitals per unit cell, this tells us that the number of the available states per band N_{as} is equal to the number of the electrons in the graphene sheet. This means the lower band shown in Fig.6 is fully filled and the last electron is filled at the Dirac points. The reason why we interest in the region near Dirac point is that its the only region where there are many available states that electrons near the Dirac cones can occupy. To conclude, we calculate the band structure of monolayer graphene in this section by using the tight-binding model. The first step is writing the trial wave function of an electron as the linear combination of the localized wave function of each electron in p_z orbitals situated at each atom. We can think that the localized wave function is the wave function of an electron in case there is no atom nearby. Second, we write the Hamiltonian where its form is determined by the basis of the trial wave function $|A\rangle, |B\rangle$. Third, we show that each Dirac point of the Brillouin zone has a different form of the Hamiltonian, which is the reason why we call them K and K' . Last, we show that the low-energy states are situated near the Dirac points. These states are important to us in the sense that it is these states that interacts with the other systems, they are free to change their states. Fig.7 shows both conduction and valence bands. Fig.8 shows the Fermi surface of the conduction band which is similar to the Fermi surface of the valence band, in this case. The only difference is the range of the energy.

2.1.2.1 Density of states

In this section, we will numerically calculate the density of states of graphene. The density of states in 2-dimensional material is defined to be the number of states per

energy per area of the material or

$$D(E) = \frac{1}{A_{mat}} \frac{dN(E)}{dE} \quad (22)$$

where $N(E)$ is the number of states that have energy below E , note that $N(E)$ can be written as a summation of a partial number of states that have energy below E as $\sum_i N_i$ where i is the band index. To find $dN(E)/dE$, we must calculate the cross-sectional area of each band E_i at energy E and $E + dE$ and use the fact that the number of states between the energy E and $E + dE$ is proportional to the difference of the cross-sectional area of the energy E and $E + dE$ or

$$dN(E) = \sum_i dN_i(E) = 2 \sum_i \frac{dA_{cross,i}(E)}{A_{state}} = \frac{A_{mat}}{2\pi^2} \sum_i \int_{BZ} dh(E_i(\mathbf{k}) - E) d^2\mathbf{k}. \quad (23)$$

where we replace A_{state} with $(2\pi/L_x)(2\pi/L_y) = 4\pi^2/A_{mat}$ and write the cross-sectional area as the intergral of the Heaviside step function h defined to be

$$h(E_i(\mathbf{k}) - E) = \begin{cases} 1, & \text{if } E_i(\mathbf{k}) - E > 0, \\ 0, & \text{if } E_i(\mathbf{k}) - E < 0. \end{cases} \quad (24)$$

By using these definitions, we can rewrite the density of states as

$$D(E) = \frac{1}{2\pi^2} \sum_i \int_{BZ} \frac{\partial h(E_i(\mathbf{k}) - E)}{\partial E} d^2\mathbf{k} \quad (25)$$

$$= \frac{\Delta k_x \Delta k_y}{2\pi^2 \Delta E} \sum_i \sum_{N_x} \sum_{N_y} (h(E_i(N_x, N_y) - E + \Delta E/2) - h(E_i(N_x, N_y) - E - \Delta E/2)) \quad (26)$$

$$= \frac{A_{BZ}}{2\pi^2 \Delta E N_{k_x} N_{k_y}} \sum_i \sum_{N_x} \sum_{N_y} \Omega(E_i(N_x, N_y) - E) \quad (27)$$

where we approximate Eq.25 to a form that can be numerically integrated using the central difference and the range of summation of each reciprocal area $\Delta k_x \Delta k_y$ is within the region of the first Brillouin zone. In Eq.27, we replace $\Delta k_x \Delta k_y$ as $A_{BZ}/N_{k_x} N_{k_y}$, where N_{k_x} and N_{k_y} are the number of grids in the k_x and k_y directions, respectively. By considering the central difference, we can write it in a more compact form as

$$\Omega(E_i(N_x, N_y) - E) = \begin{cases} 1, & \text{if } |E_i(N_x, N_y) - E| < \Delta E/2, \\ 0, & \text{if } |E_i(N_x, N_y) - E| > \Delta E/2. \end{cases} \quad (28)$$

It's a bit tricky to define the grids of N_x and N_y . Because the shape of the first Brillouin zone of graphene is hexagonal, choosing the region for the integration to be the first Brillouin zone is a bit complicate task as one has to the range of integration along k_x for each constant k_y . This problem can be solved by choosing another the region of integration shown in Fig.9. The density of states of graphene calculating according to the method above is shown in Fig.10. The density of states near the Dirac points is linear because the dispersion relation near those points is linear, Eq.19. This means the number of states between energy E and $E + dE$ near the Dirac points is

$$dN(E) = \sum_i dN_i(E) = 2 \frac{dA_{cross}(E)}{A_{state}} = 2 \frac{2\pi|\mathbf{q}||d\mathbf{q}|}{4\pi^2/A_{mat}} = \frac{A_{mat}}{\pi} \frac{4EdE}{3t^2a^2} \quad (29)$$

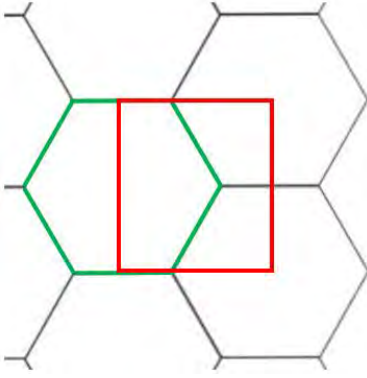


Figure 9: The first Brillouin zone is the region surrounded by the green lines. In this work, we choose the region to calculate the density of states to be the region in the region surrounded by the red lines. These two regions are equivalent; they have the same area.

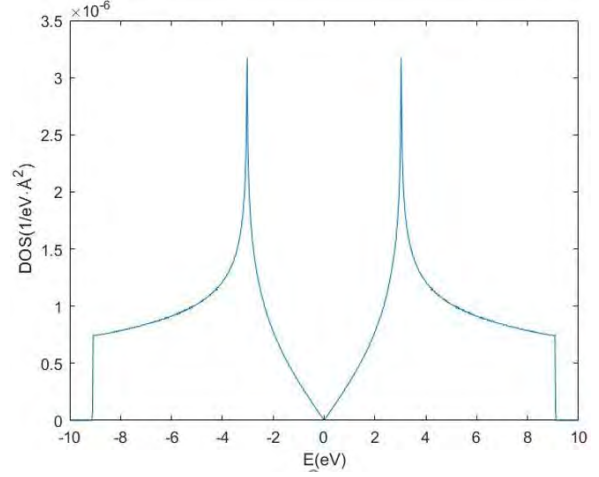


Figure 10: The density of states of graphene calculated by using $N_x = N_y = 300$. The density of states grows proportionally to the energy of electrons when $|E| \ll 1\text{eV}$, which comes from the fact that the dispersion relation near the Dirac points is linear. We can reduce the error by increasing N_x and N_y .

where $i = 1, 2$ but we need to calculate only one term as the cross-sectional area only comes from one of the bands and \mathbf{q} is the vector measured from the Dirac points, Fig.5. By replacing the dispersion relation near the Dirac points from Eq.19 in Eq.29, the density of states of graphene near the Dirac points is

$$D(E) = \frac{1}{A_{mat}} \frac{dN(E)}{dE} = \frac{4E}{3\pi t^2 a^2} \quad (30)$$

which is linear in E as seen in Fig.10.

2.1.3 Bilayer graphene

For bilayer graphene, the unit cell of AB-stacked bilayer graphene is shown in Fig.11. As you can see from the Figure, there are four carbon atoms in each unit cell which means there are four sub-lattices named A1, B1, A2, B2 in each unit cell. To calculate the band structure of bilayer graphene, we use the same strategy using to calculate the band structure of monolayer graphene. We start by writing the trial wave function of an electron as

$$|\mathbf{k}\rangle = \sum_{\mathbf{r}_{A1}} \phi_{\mathbf{r}_{A1}, \mathbf{k}} |\mathbf{r}_{A1}\rangle + \sum_{\mathbf{r}_{B1}} \phi_{\mathbf{r}_{B1}, \mathbf{k}} |\mathbf{r}_{B1}\rangle + \sum_{\mathbf{r}_{A2}} \phi_{\mathbf{r}_{A2}, \mathbf{k}} |\mathbf{r}_{A2}\rangle + \sum_{\mathbf{r}_{B2}} \phi_{\mathbf{r}_{B2}, \mathbf{k}} |\mathbf{r}_{B2}\rangle \quad (31)$$

$$= c_{A1} \sum_{\mathbf{r}_{A1}} \frac{e^{i\mathbf{r}_{A1} \cdot \mathbf{k}}}{\sqrt{N_{uc}}} |\mathbf{r}_{A1}\rangle + c_{B1} \sum_{\mathbf{r}_{B1}} \frac{e^{i\mathbf{r}_{B1} \cdot \mathbf{k}}}{\sqrt{N_{uc}}} |\mathbf{r}_{B1}\rangle + c_{A2} \sum_{\mathbf{r}_{A2}} \frac{e^{i\mathbf{r}_{A2} \cdot \mathbf{k}}}{\sqrt{N_{uc}}} |\mathbf{r}_{A1}\rangle + c_{B2} \sum_{\mathbf{r}_{B2}} \frac{e^{i\mathbf{r}_{B2} \cdot \mathbf{k}}}{\sqrt{N_{uc}}} |\mathbf{r}_{B2}\rangle \quad (32)$$

$$= c_{A1} |A1, \mathbf{k}\rangle + c_{B1} |B1, \mathbf{k}\rangle + c_{A2} |A2, \mathbf{k}\rangle + c_{B2} |B2, \mathbf{k}\rangle. \quad (33)$$

We use this trial wave function because the carbon atoms around each sub-lattice are different. As you can see, Thus, the probability of finding an electron in each sub-lattice

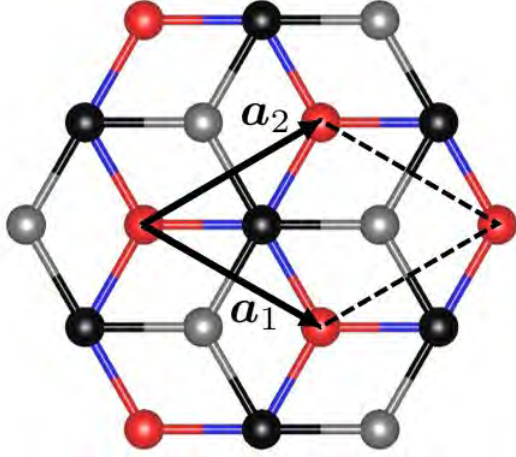


Figure 11: The unit cell of bilayer graphene is the region in the black lines. There are four sub-lattices in each unit cell which are A1(red), B1(blue), A2(black), B2(grey). For AB-stacked bilayer graphene(which is a more stable pattern), the sublattices B1 will align with the sublattices A2.

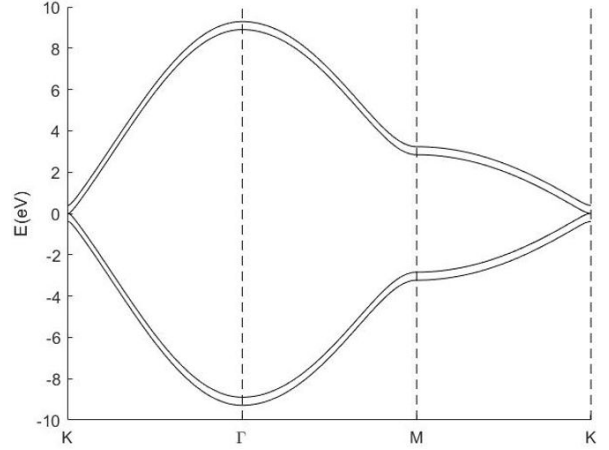


Figure 12: The band structure of bilayer graphene is shown here. The four bands arise from the fact that our wave function has four basis $|A1\rangle, |B1\rangle, |A2\rangle, |B2\rangle$. The two bands touch each other at the 6 Dirac points called K' and K . We use $t = 3.03\text{eV}$ and $\gamma = 0.39\text{eV}$ for these bands.

may be different. Next, we can use the basis of the trial wave function to determine the form of the Hamiltonian in this basis as

$$H_{bi,low}^{eff} = \begin{bmatrix} \langle A1, \mathbf{k} | H | A1, \mathbf{k} \rangle & \langle A1, \mathbf{k} | H | B1, \mathbf{k} \rangle & \langle A1, \mathbf{k} | H | A2, \mathbf{k} \rangle & \langle A1, \mathbf{k} | H | B2, \mathbf{k} \rangle \\ \langle B1, \mathbf{k} | H | A1, \mathbf{k} \rangle & \langle B1, \mathbf{k} | H | B1, \mathbf{k} \rangle & \langle B1, \mathbf{k} | H | A2, \mathbf{k} \rangle & \langle B1, \mathbf{k} | H | B2, \mathbf{k} \rangle \\ \langle A2, \mathbf{k} | H | A1, \mathbf{k} \rangle & \langle A2, \mathbf{k} | H | B1, \mathbf{k} \rangle & \langle A2, \mathbf{k} | H | A2, \mathbf{k} \rangle & \langle A2, \mathbf{k} | H | B2, \mathbf{k} \rangle \\ \langle B2, \mathbf{k} | H | A1, \mathbf{k} \rangle & \langle B2, \mathbf{k} | H | B1, \mathbf{k} \rangle & \langle B2, \mathbf{k} | H | A2, \mathbf{k} \rangle & \langle B2, \mathbf{k} | H | B2, \mathbf{k} \rangle \end{bmatrix}. \quad (34)$$

The upper-diagonal and lower-diagonal blocks in the above Hamiltonian represents the tunnelling between the sites in the same layer, which we have calculated earlier. Thus, we can replace them with the Hamiltonian of the monolayer graphene in those blocks. For the off-diagonal blocks, we will approximate that the tunnelling integral between layers, or the chance of an electron to tunnelling from a specific site to another site, will vanish if those two sites are not aligned. This means only $\langle B1, \mathbf{k} | H | A2, \mathbf{k} \rangle$ is non-zero here. If we let the tunnelling integral between A2 and B1 to be γ where the distance between those two sites must equal to the interlayer distance, we can show that

$$\langle B1, \mathbf{k} | H | A2, \mathbf{k} \rangle = \sum_{\mathbf{r}_{B1}} \sum_{\mathbf{r}_{A2}} \frac{e^{i(\mathbf{r}_{A2} - \mathbf{r}_{B1}) \cdot \mathbf{k}}}{N_{uc}} \langle \mathbf{r}_{B1} | H | \mathbf{r}_{A2} \rangle = \sum_{\mathbf{r}_{B1}} \frac{e^{i\mathbf{L} \cdot \mathbf{k}} \gamma}{N_{uc}} = e^{i\mathbf{L} \cdot \mathbf{k}} \gamma = \gamma \quad (35)$$

where \mathbf{L} is the vectors pointing from each site B1 to the site A2 above it, its magnitude is the interlayer distance which is 3.35 \AA . As you can see from Eq.35, we set $k_z = 0$. This is because the next k_z from 0, or Δk_z , is $2\pi/|\mathbf{L}|$ which too large compared to Δk_x and Δk_y . In other words, electrons can't go to those high energy states. So, electrons can only situate in the states where $k_z = 0$. From now on, we will set $k_z = 0$. If you insist on leaving k_z in the Hamiltonian, you will get the same result as setting k_z to zero anyway. It's not because the Hamiltonian doesn't depend on k_z . It's because we

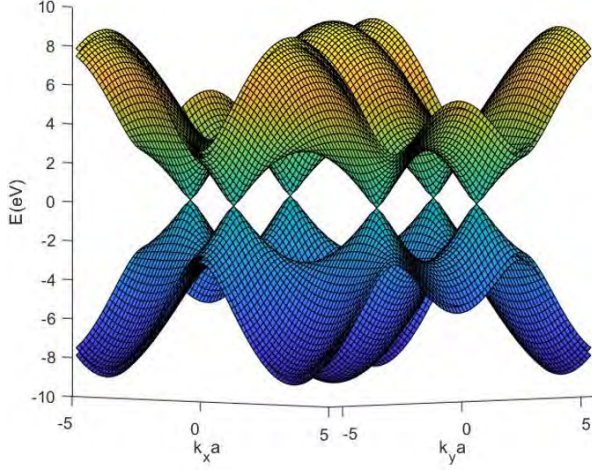


Figure 13: The valence and conduction bands. There are 4 bands in this figure.

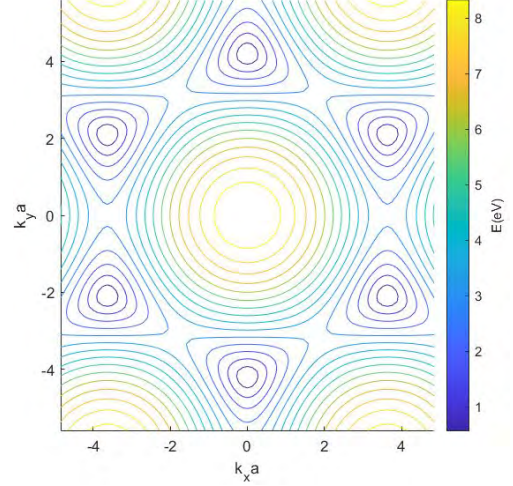


Figure 14: The Fermi surface of the conduction band of bilayer graphene.

approximate the Hamiltonian by keeping only the tunnelling between the sites B1 and A2. If we keep the rest tunnelling between other sites, k_z will appear in the Hamiltonian. Now by replacing the rest terms on the Hamiltonian, we get

$$H_{bi,low}^{eff} = \begin{bmatrix} 0 & -tf(\mathbf{k}) & 0 & 0 \\ -tf(\mathbf{k})^* & 0 & \gamma & 0 \\ 0 & \gamma & 0 & -tf(\mathbf{k}) \\ 0 & 0 & -tf(\mathbf{k})^* & 0 \end{bmatrix}. \quad (36)$$

Diagonalizing the Hamiltonian gives the band structure of bilayer graphene shown in Fig.12. We plot the band structure along the first Brillouin zone defined in Fig.5 because the lattice vectors of bilayer graphene and monolayer graphene are the same which yields the same Brillouin zone. From Eq.36, we can show that

$$E_k = \pm \sqrt{t^2|f(\mathbf{k})|^2 + \frac{\gamma^2}{2} \pm \frac{\gamma^2}{2} \sqrt{1 + \frac{4t^2|f(\mathbf{k})|^2}{\gamma^2}}} = \pm \left(\sqrt{\frac{\gamma^2}{4} + t^2|f(\mathbf{k})|} \pm \frac{\gamma}{2} \right). \quad (37)$$

The bottom of the energy bands, near the Dirac cones, can be approximated by replacing, see Eq.19,

$$|f(\mathbf{K} + \mathbf{q})| \rightarrow \frac{\sqrt{3}a}{2} |\mathbf{q}| \quad (38)$$

which yields

$$E_k^{low}(\mathbf{q}) \approx \pm \frac{\gamma}{2} \left(1 + \frac{2t^2|f(\mathbf{K} + \mathbf{q})|}{\gamma^2} \pm 1 \right) \sim \frac{3t^2a^2}{4\gamma} |\mathbf{q}|^2 \quad (39)$$

which is valid when $2t|f(\mathbf{K} + \mathbf{q})| \ll \gamma$. Because the relation between the energy and the crystal momentum is quadratic, see the regions near Dirac cones in Fig.13, the behaviour of electrons in the bilayer graphene near the bottom of energy bands are not

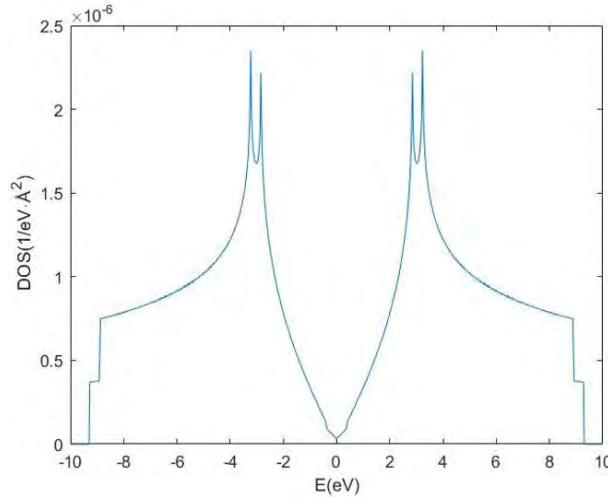


Figure 15: The shape of this DOS is similar to the DOS of graphene. There are more peaks in the case of bilayer graphene.

the same as low energy electrons in graphene. The electrons in bilayer graphene are similar to electron gas having effective mass equal to $2\gamma/3t^2a^2\hbar^2$. The Fermi surface near the Dirac cones of bilayer graphene, shown in Fig.14, is similar to the Fermi surface near the Dirac cones of graphene, shown in Fig.8, because the shape of band structure of bilayer graphene near the Dirac cones is paraboloid, which means the cross-section of each low energy level will be circle. The difference between dispersion relations near the Dirac cones of single layer graphene and bilayer graphene also leads to the difference filling factors in quantum Hall effects[10][11][12].

2.1.3.1 Density of states

We use the method used in calculating the density of states of graphene to calculate the density of states of bilayer graphene. Fig.15 shows the density of states of electrons in bilayer graphene.

2.2 Twisted bilayer graphene

2.2.1 Crystal structure of twisted bilayer graphene

Twisted bilayer graphene is actually bilayer graphene where the two layers are twisted by angle θ . When two graphenes are twisted with respect to each other, there will be some angles where supercells, a periodic crystal, appear. In other words, it is the twist angles which cause stackings of sub-lattices A2 on B1 periodically along the plane. Those angles are called commensurate angles where other angles that don't produce a crystal are called non-commensurate angles. Because the band theory works in the case where there is a periodic crystal, we want to know which angles are commensurate. To derive the formula for calculating the commensurate angles, we need to know that each carbon atom has an axis of 6-fold symmetry, Fig.16, perpendicular to its plane. This means rotating graphene by 60° is equivalent to do nothing as it will look the same, you might ask that the colours are changed, but colours have nothing to do with the crystal structure. Graphene also has mirror planes perpendicular to its

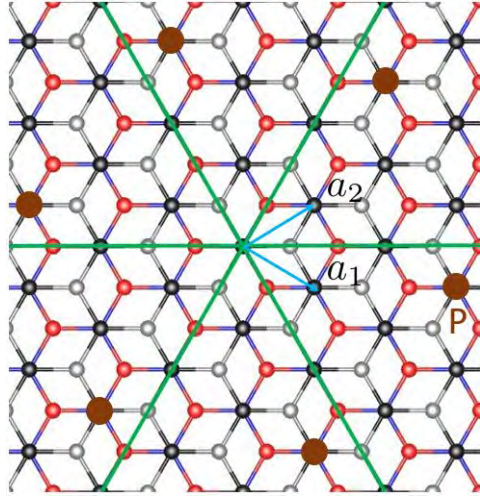


Figure 16: By choosing a point P which is equivalent to the point at the origin, we can generate more five points from rotating the point P by 60° .

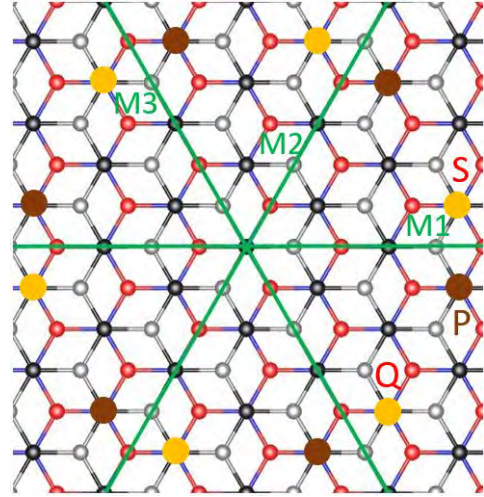


Figure 17: By using the mirror planes, we can generate more six points (yellow) which can be regarded as points in another layer.

plane, along the direction shown in Fig.17. In order to find the commensurate angles, we must choose one of carbon atoms to be an axis of the rotation. Conventionally, we want to choose a carbon atom in a sub-lattice B1 or A2. In this case, we choose the carbon atom in the middle of the intersection shown in Fig.16. Next, we must find another carbon atom which is equivalent to the first chosen atom. We do this because we want to use this atom to determine the superstructure by rotating the atom, around the axis, to superimpose another carbon atom which has the same distance from the origin of the rotation. In our case, we choose the carbon atom at the point P to be rotated. The next problem is how can we determine the number of carbon atoms which has the same distance from the origin equal to the distance between the point P and the origin. We can solve this problem by using the fact that each carbon atom in graphene has an axis of 6-fold symmetry perpendicular to it. Thus, we can generate the other five carbon atoms which have the same distances from the origin by rotating the graphene 60° around the origin five times. The result is shown in Fig.16. We can also generate the rest six carbon atoms coloured in yellow which have the same distance from the origin as the point P by using the mirror planes to reflect the first six carbon atoms. From point P, we can generate 11 carbon atoms by using the 6-fold symmetry and mirror planes. The result is shown in Fig.17. Now, if we rotate the point P to the point S, the supercell lattice vectors will be determined by the vector pointing from the origin to the point S. We can generate another supercell lattice vector by rotating this vector by 60° . If we rotate the point Q to the point P, the supercell lattice vectors will be determined by the vector pointing from the origin to the point P. Another supercell lattice vector is generated according to the method above. If the coordinate of the point P is

$$P = na_1 + ma_2 \quad (40)$$

where $n > m > 0$, we can generate the point S by reflecting the point P across the line M1. This task can be simplified by creating a reflection matrix T_1 , which will reflect a given point with respect to the line M1. For other mirrors, their reflection operators are

noted as T_i where $i = 1, 2, 3$. From Fig.16, it's clear that

$$T_1(\mathbf{a}_1) = \mathbf{a}_2 \quad \text{and} \quad T_1(\mathbf{a}_2) = \mathbf{a}_1. \quad (41)$$

By using the fact that this operator is linear in its argument, we can show that the coordinate of the point S can be written as

$$S = T_1(P) = nT_1(\mathbf{a}_1) + mT_1(\mathbf{a}_2) = n\mathbf{a}_2 + m\mathbf{a}_1. \quad (42)$$

We can also generate the point Q by doing the three following steps. First, we use the reflection operator T_2 to reflect the point Q across the line M2. Next, we use the inversion operator to inverse that point. This is equivalent to adding the minus sign to a point we want to inverse. Last, we use the reflection operator T_3 to reflect the point Q across the line M3. These steps for generating Q can be concluded as

$$Q = T_3(-T_2(S)). \quad (43)$$

From Fig.16, we can see that

$$T_2(\mathbf{a}_2) = \mathbf{a}_2 - \mathbf{a}_1 \quad , \quad T_2(\mathbf{a}_2 - \mathbf{a}_1) = \mathbf{a}_2 \quad (44)$$

and

$$T_3(-\mathbf{a}_1) = \mathbf{a}_2 - \mathbf{a}_1 \quad , \quad T_3(\mathbf{a}_2 - \mathbf{a}_1) = -\mathbf{a}_1. \quad (45)$$

Because the operator T_2 is linear, we can rewrite Eq.44 as

$$T_2(\mathbf{a}_1) = -\mathbf{a}_1 \quad , \quad T_2(\mathbf{a}_2) = -\mathbf{a}_1 + \mathbf{a}_2. \quad (46)$$

The same procedure can be used to rewrite Eq.45 as

$$T_3(\mathbf{a}_1) = \mathbf{a}_1 - \mathbf{a}_2 \quad , \quad T_3(\mathbf{a}_2) = -\mathbf{a}_2. \quad (47)$$

By using the properties of the reflection matrices T_2 and T_3 written in Eq.45 and 46, it's straightforward to show that

$$Q = T_3(-T_2(S)) = T_3(-nT_2(\mathbf{a}_2) - mT_2(\mathbf{a}_1)) = (n+m)\mathbf{a}_1 - m\mathbf{a}_2 \quad (48)$$

Now that we have all the coordinates of P, Q and S, rotating the point P to the point S would yield the supercell lattice vectors defined by the vector pointing from the origin to the point S or \mathbf{R}_1 . Another supercell lattice vector \mathbf{R}_2 can be obtained by rotating \mathbf{R}_1 by 60° anti-clockwise. This is equivalent to use the operator $-T_2T_3$ on P. In this case, the supercell lattice vectors when we rotate the point P to S are

$$\mathbf{R}_1 = m\mathbf{a}_1 + n\mathbf{a}_2 \quad \text{and} \quad \mathbf{R}_2 = -T_2(T_3(\mathbf{R}_1)) = -n\mathbf{a}_1 + (n+m)\mathbf{a}_2 \quad (49)$$

where the twist angle calculating using the cosine law is

$$\cos \theta(m,n) = \frac{|S|^2 + |P|^2 - |S-P|^2}{2|S||P|} = 1 - \frac{|S-P|^2}{2|P|^2} = \frac{3(m+n)^2 - (n-m)^2}{3(m+n)^2 + (n-m)^2} \quad (50)$$

where $\mathbf{a}_1 = a(\sqrt{3}/2, -1/2)$ and $\mathbf{a}_2 = a(\sqrt{3}/2, 1/2)$. If we choose to rotate the point Q to the point P, the supercell lattice vectors \mathbf{R}_1 is equal to the vector that points from the

origin to P. rotating $\tilde{\mathbf{R}}_1$ by 60° anti-clockwise with respect to the origin yields $\tilde{\mathbf{R}}_2$. This is equivalent to use the operator $-T_2T_3$ on P. Another supercell lattice vector is the vector pointing from the origin to the point P or $\tilde{\mathbf{R}}_2$. Thus, the supercell lattice vectors in this case are

$$\tilde{\mathbf{R}}_1 = q\mathbf{a}_1 + p\mathbf{a}_2 \quad \text{and} \quad \tilde{\mathbf{R}}_2 = -T_2(T_3(\tilde{\mathbf{R}}_1)) = -p\mathbf{a}_1 + (p+q)\mathbf{a}_2 \quad (51)$$

,note we change $n \rightarrow q$ and $m \rightarrow p$ to avoid the confusion later. The twist is

$$\cos \theta'(p, q) = \frac{|P|^2 + |Q|^2 - |P-Q|^2}{2|P||Q|} = 1 - \frac{|P-Q|^2}{2|Q|^2} = \frac{4q^2 + 4pq + p^2}{3(p+q)^2 + (p-q)^2}. \quad (52)$$

There formulas in Eq.50 and 52 can generate the same set of commensurate angles. In other words, there are always integers (m, n) and (p, q) for a given commensurate angle θ_0 or

$$\cos \theta_0 = \cos \theta(m, n) = \cos \theta(p, q) \quad (53)$$

. But there is only one of them that produces the shorter supercell lattice vectors for each θ_0 . This can be seen clearly by transforming $n-m=r$ and $q-p=s$. Now, we can rewrite Eq.53 using these new variables as

$$\cos \theta_0 = \frac{3m^2 + 3mr + r^2/2}{3m^2 + 3mr + r^2} = \frac{3(m+r/2)^2 - (r/2)^2}{3(m+r/2)^2 + (r/2)^2} \rightarrow \tan \theta_0/2 = \frac{1}{\sqrt{3}} \left(1 + \frac{2m}{r} \right) \quad (54)$$

and

$$\cos \theta_0 = \frac{3p^2/2 + 3ps + s^2}{3p^2 + 3ps + s^2} = \frac{3(3p/2 + s)^2 - (3p/2)^2}{3(3p/2 + s)^2 + (3p/2)^2} \rightarrow \tan \theta_0/2 = \frac{1}{\sqrt{3}} \left(1 + \frac{2s}{3p} \right). \quad (55)$$

By comparing Eq.54 and 55, we can see that the relation between (m, r) and (s, p) for each commensurate angle θ_0 is

$$\frac{m}{r} = \frac{s}{3p}. \quad (56)$$

For a commensurate angle generated when $m=s$ and $r=3p$, the norm of the supercell lattice vector from (m, r) is longer than the norm of the supercell lattice vector from (s, p) which we can be shown as, by using Eq.49 and 51,

$$\mathbf{R}_1 \cdot \mathbf{R}_1 > \tilde{\mathbf{R}}_2 \cdot \tilde{\mathbf{R}}_2 \quad (57)$$

$$(r+s)^2|\mathbf{a}_1|^2 + 2s(r+s)\mathbf{a}_1 \cdot \mathbf{a}_2 + s^2|\mathbf{a}_2|^2 > (r/3)^2|\mathbf{a}_1|^2 + 2(r/3)(s+r/3)\mathbf{a}_1 \cdot \mathbf{a}_2 + (s+r/3)^2|\mathbf{a}_2|^2 \quad (58)$$

$$(r+s)^2 + s(r+s) + s^2 > (r/3)^2 + (r/3)(s+r/3) + (s+r/3)^2 \quad (59)$$

$$2r^2/3 + 2rs + 2s^2 > 0 \quad (60)$$

where we use $\tilde{\mathbf{R}}_2$ instead of using $\tilde{\mathbf{R}}_1$ because their lengths are equal but $\tilde{\mathbf{R}}_2$ has a simple form. Thus, if we want to calculate the commensurate angles by using Eq.54, we must use

$$\tilde{\mathbf{R}}_1 = \left(m + \frac{r}{3} \right) \mathbf{a}_1 + \frac{r}{3} \mathbf{a}_2 \quad \text{and} \quad -\frac{r}{3} \mathbf{a}_1 + \left(m + \frac{2r}{3} \right) \mathbf{a}_2 \quad (61)$$

from Eq.51 as the supercell lattice vectors when r can be divided by 3 because their norms are shorter than the norms of \mathbf{R}_1 and \mathbf{R}_2 . Note that we replace q by $s+p$ and

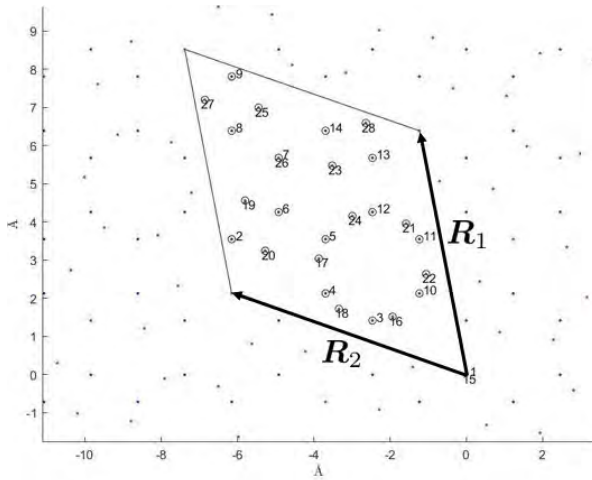


Figure 18: For $m = r = 1$, there are 28 sites in each supercell where \mathbf{R}_1 and \mathbf{R}_2 are supercell lattice vectors.

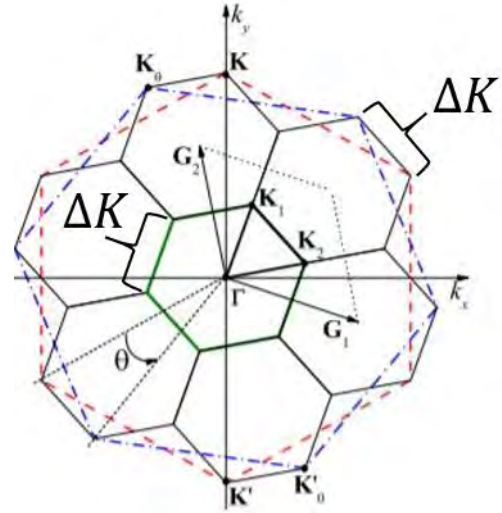


Figure 19: The first Brillouin zone of the supercell is much smaller than the first Brillouin zone of each layer. The distance between the nearest Dirac points is equal to the length of each side of the first Brillouin zone of the supercell. This figure is adapted from [9].

p by $r/3$ in Eq.61. When r can't be divided by 3, we have $r = p$ and $s = 3m$ for each commensurate angle θ_0 . It can be shown that the norm of \mathbf{R}_1 is shorter than the norm of \mathbf{R}_2 in this case. Thus, we must use the supercell lattice vectors from Eq.49 or

$$\mathbf{R}_1 = m\mathbf{a}_1 + (m+r)\mathbf{a}_2 \quad \text{and} \quad \mathbf{R}_2 = -(m+r)\mathbf{a}_1 + (2m+r)\mathbf{a}_2 \quad (62)$$

where we replace n by $m+r$. To conclude, we will use Eq.54

$$\cos \theta(n, m) = \frac{3m^2 + 3mr + r^2/2}{3m^2 + 3mr + r^2} \quad (63)$$

to generate the commensurate angles. If $\text{mod}(r,3) = 0$, the supercell lattice vectors are, from Eq.61,

$$\mathbf{R}_1 = \left(m + \frac{r}{3}\right)\mathbf{a}_1 + \frac{r}{3}\mathbf{a}_2 \quad \text{and} \quad \mathbf{R}_2 = -\frac{r}{3}\mathbf{a}_1 + \left(m + \frac{2r}{3}\right)\mathbf{a}_2. \quad (64)$$

if $\text{mod}(r,3) \neq 0$, the supercell lattice vectors are, from Eq.62

$$\mathbf{R}_1 = m\mathbf{a}_1 + (m+r)\mathbf{a}_2 \quad \text{and} \quad \mathbf{R}_2 = -(m+r)\mathbf{a}_1 + (2m+r)\mathbf{a}_2. \quad (65)$$

Figure 18 shows the supercell with $m = r = 1$. The first Brillouin zone of the supercell, which can be calculated from \mathbf{R}_1 and \mathbf{R}_2 , in this case, is shown in Fig.19. As you can see, the size of the first Brillouin zone of the supercell is smaller than the first Brillouin zone of each layer. This should be clear from the fact that the length of the supercell lattice vectors is larger than the distance between each sublattice. The number of the sites in each supercell N_{sc} , shown in Fig.18, can be calculated from the fact that the area of the supercell A_{sc} can be written $A_{uc}N_{uc}$ where A_{uc} is the area of the unit cell

of bilayer graphene and N_{uc} is the number of the unit cells of bilayer graphene in the supercell. Thus, the number of sites in each supercell is

$$N_{sc} = 4 \frac{A_{sc}}{A_{uc}N_{uc}} = 4 \frac{|\mathbf{R}_1 \times \mathbf{R}_2|}{A_{uc}N_{uc}} \quad (66)$$

where the factor four comes from the fact that there are four sites in each unit cell of bilayer graphene. By using the supercell lattice vectors from Eq.64 and Eq.65, we can show that when $\text{mod}(r,3) \neq 0$

$$N_{sc} = 4(3m^2 + 3mr + r^2) \quad (67)$$

and when $\text{mod}(r,3) = 0$

$$N_{sc} = 4(m^2 + mr + r^2/3). \quad (68)$$

2.2.2 Continuum model of twisted bilayer graphene

We follow the method used in calculating the band structure of monolayer graphene and bilayer graphene. First, we start by constructing the trial wave function of an electron in twisted bilayer graphene which is a linear combination of wave functions from each sub-lattice. The wave function of an electron of a n sub-lattice from layer $s(1,2)$ can be written as

$$|n, s, \mathbf{k}\rangle = \sum_{\mathbf{r}_n} \frac{e^{i\mathbf{r}_n \cdot \mathbf{k}}}{\sqrt{N_{sc}}} |\mathbf{r}_n, s\rangle. \quad (69)$$

Thus, the trial wave function of an electron in twisted bilayer graphene is

$$|\mathbf{k}\rangle = \sum_s \sum_n c_{n,s} |n, s, \mathbf{k}\rangle. \quad (70)$$

A component of the Hamiltonian of twisted bilayer graphene is given by

$$\langle m, s_i, \mathbf{k} | H | n, s_j, \mathbf{k} \rangle = \sum_{\mathbf{r}_n} \sum_{\mathbf{r}_m} \frac{e^{i(\mathbf{r}_n - \mathbf{r}_m) \cdot \mathbf{k}}}{N_{sc}} \langle \mathbf{r}_n, s_i | H | \mathbf{r}_m, s_j \rangle. \quad (71)$$

We can rewrite \mathbf{r}_n , the position of a point in a sub-lattice n , as

$$\mathbf{r}_n = \mathbf{R} + \mathbf{v}_n \quad (72)$$

where \mathbf{R} is a vector pointing to one of the lattice points of supercell and \mathbf{v}_n is a position of the lattice point n relative to each supercell. Now, Eq.64 can be rewritten as

$$\langle m, s_i, \mathbf{k} | H | n, s_j, \mathbf{k} \rangle = \sum_{\mathbf{R}} \sum_{\mathbf{R}'} \frac{e^{i(\mathbf{R} + \mathbf{v}_n - \mathbf{R}' - \mathbf{v}_m) \cdot \mathbf{k}}}{N_{sc}} \langle \mathbf{R} + \mathbf{v}_n, s_i | H | \mathbf{R}' + \mathbf{v}_m, s_j \rangle. \quad (73)$$

If we change to the basis from $|\mathbf{R} + \mathbf{v}_n, s_i\rangle \rightarrow e^{i\mathbf{v}_n \cdot \mathbf{k}} |\mathbf{R} + \mathbf{v}_n, s_i\rangle$, Eq.66 can be written as

$$\langle m, s_i, \mathbf{k} | H | n, s_j, \mathbf{k} \rangle = \sum_{\mathbf{R}} \sum_{\mathbf{R}'} \frac{e^{i(\mathbf{R} - \mathbf{R}') \cdot \mathbf{k}}}{N_{sc}} \langle \mathbf{R} + \mathbf{v}_n, s_i | H | \mathbf{R}' + \mathbf{v}_m, s_j \rangle. \quad (74)$$

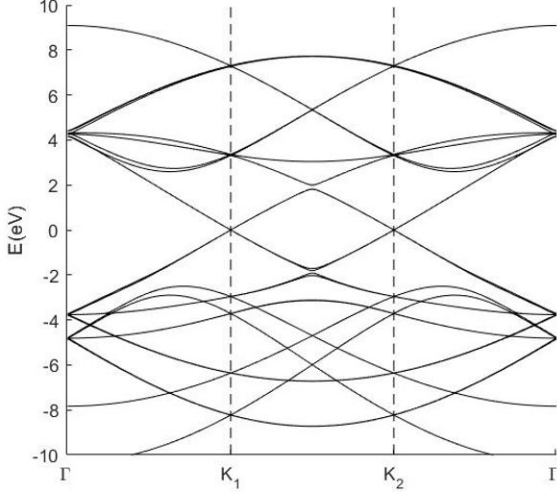


Figure 20: The band structure of twisted bilayer graphene for $m = r = 1$ plot along $\Gamma \rightarrow K_1 \rightarrow K_2 \rightarrow \Gamma$, see Fig.18

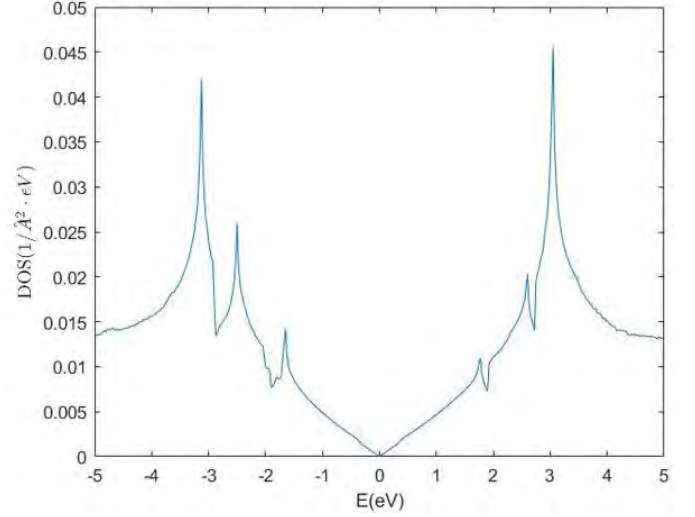


Figure 21: Density of states of electrons in twisted bilayer graphene for $m = r = 1$.

For each \mathbf{R}' , we can see that summation over all supercells in the lattice yields the same result whether there is a vector \mathbf{R}' or not. For simplicity, we will set $\mathbf{R}' = 0$ in the Eq.74. Thus, we will get

$$\langle m, s_i, \mathbf{k} | H | n, s_j, \mathbf{k} \rangle = \sum_{\mathbf{R}} \sum_{\mathbf{R}'} \frac{e^{i\mathbf{R} \cdot \mathbf{k}}}{N_{sc}} \langle \mathbf{R} + \mathbf{v}_n, s_i | H | \mathbf{v}_m, s_j \rangle. \quad (75)$$

By using the continuum model which approximates the tunnelling amplitude to a continuous function of the distance between two sites and the fact that the number of vectors \mathbf{R}' is equal to the number of supercell N_{sc} , we get

$$\langle m, s_i, \mathbf{k} | H | n, s_j, \mathbf{k} \rangle = \sum_{\mathbf{R}} e^{i\mathbf{R} \cdot \mathbf{k}} \tau(\mathbf{R} + \mathbf{v}_n - \mathbf{v}_m) = \sum_{\mathbf{R}} e^{i\mathbf{R} \cdot \mathbf{k}} \tau(\mathbf{v}_m - \mathbf{R} - \mathbf{v}_n). \quad (76)$$

where τ is the tunnelling function which continuously depends on the distance between two sites. In this works, we use a tunnelling function

$$t(s) = A e^{-(s-h)/B} \frac{\hbar^2}{s^2} \quad (77)$$

where s is the distance between two sites. if $s = h = 3.35 \text{ \AA}$, the distance between two layers, we know that $t(h) = 0.39 \text{ eV}$. If $s = d = 1.42 \text{ \AA}$, the distance between carbon atoms, we know that $t(d) = 3.03 \text{ eV}$. By using this information, we can fit the parameters A and B which are equal to 0.39 eV and 0.27 \AA , respectively. If the two sites n and m are on the same layer, we will consider only the tunnelling between nearest neighbour sites. Thus, we can approximate Eq.76 as

$$\langle m, s_i, \mathbf{k} | H | n, s_j, \mathbf{k} \rangle = \sum_{\mathbf{R}} e^{i\mathbf{R} \cdot \mathbf{k}} \tau(\mathbf{R} + \mathbf{v}_n - \mathbf{v}_m) = \sum_{\mathbf{R}} e^{i\mathbf{R} \cdot \mathbf{k}} t \delta(|\mathbf{v}_m - \mathbf{R} - \mathbf{v}_n| - d) \quad (78)$$

where δ is the Kronecker delta and d is the distance between carbon atoms. The band structure and Fermi surface of twisted bilayer graphene when $m = r = 1$ is shown in Fig.20 and 22.

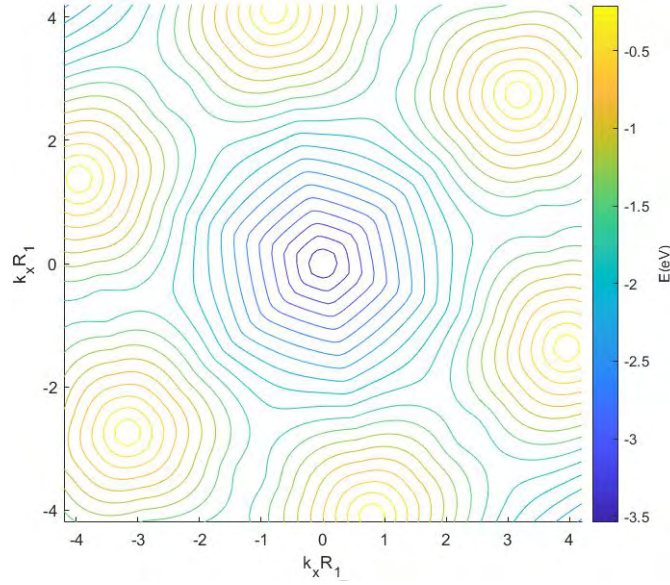


Figure 22: The Fermi surface of twisted bilayer graphene is similar to the Fermi surface of graphene and bilayer graphene. It's rotated in the clockwise direction.

2.2.2.1 Density of states

The density of states of electrons in twisted bilayer graphene for $m = r = 1$ is shown in Fig.21.

2.2.3 Low energy regime of twisted bilayer graphene

In this section, we will derive the band structure of twisted bilayer graphene in low energy regime. The main idea is that only electrons in the low energy states correspond to this regime. In the previous section, the trial wave function of an electron is written as a linear combination of localized wavefunctions of electrons in the same sub-lattice. Then, we calculate the tunneling amplitude or the probability of tunneling between sub-lattices. The momentum \mathbf{k} in the previous section is measured with respect to the center of the first Brillouin zone of the supercell but not the center of the first Brillouin zone of each unit cell of graphene. Thus, it's not clear whether the momentum states $|n, s, \mathbf{k}\rangle$ in the previous section refers to the low energy state. This suggests us to write a momentum state \mathbf{k} of an electron where \mathbf{k} is measured with respect to the center of the first Brillouin zone of each unit cell of graphene. With this definition of the momentum state \mathbf{k} , we can easily denote the region where \mathbf{k} corresponds to a low energy state, the state near Dirac points. Next, we can create a momentum state \mathbf{k} of an electron from each layer according to the new definition of the momentum state as

$$|\psi_{\mathbf{k}, \alpha}^1\rangle = \frac{1}{\sqrt{N_{uc}}} \sum_{\mathbf{R}} e^{i\mathbf{k}(\mathbf{R} + \boldsymbol{\tau}_\alpha)} |\mathbf{R} + \boldsymbol{\tau}_\alpha\rangle, \quad (79)$$

$$|\psi_{\mathbf{p}, \beta}^2\rangle = \frac{1}{\sqrt{N_{uc}}} \sum_{\mathbf{R}'} e^{i\mathbf{p}(\mathbf{R}' + \boldsymbol{\tau}'_\beta)} |\mathbf{R}' + \boldsymbol{\tau}'_\beta\rangle. \quad (80)$$

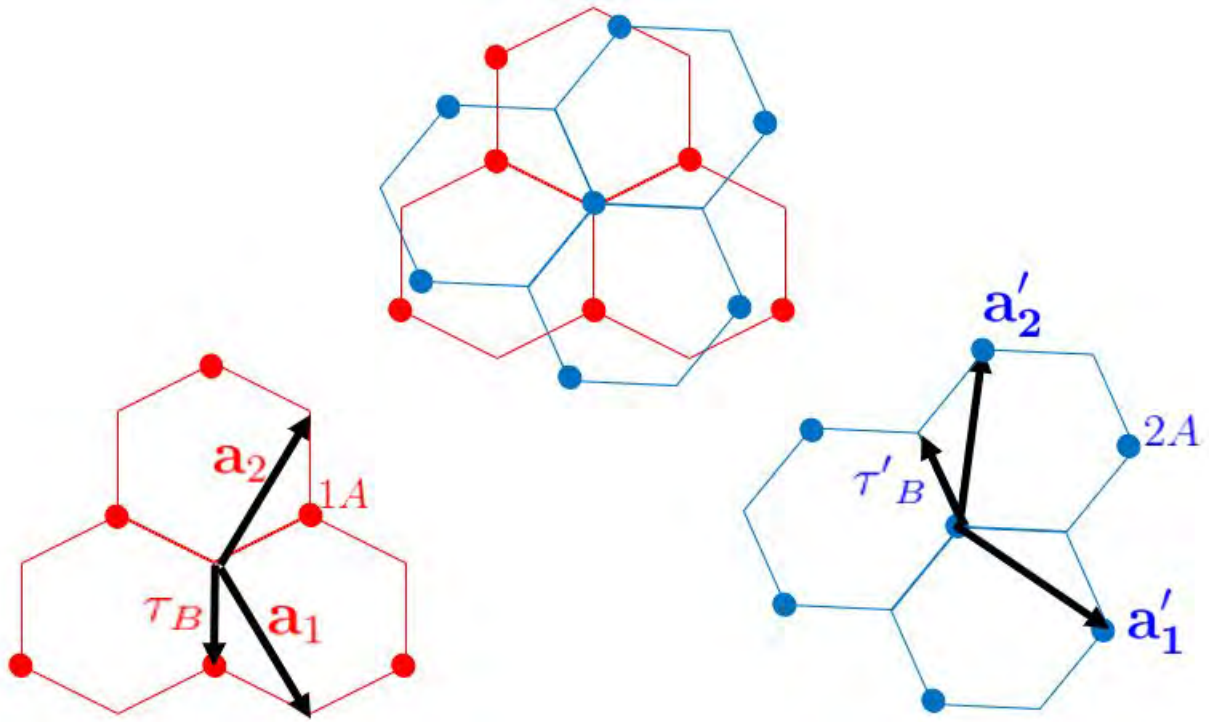


Figure 23: The notation of variables of the real lattice used in this model. The red layer is unrotated while the blue layer is rotated. carbon atoms B1 is below carbon atoms A2. The dots signify A-sublattices in both layers.

where

- \mathbf{k} = a momentum state \mathbf{k} measured from the center of the first Brillouin zone of the layer 1,
- \mathbf{p} = a momentum state \mathbf{p} measured from the center of the first Brillouin zone of the layer 2,
- α, β = a sublattice(A or B),
- N_{uc} = the number of unit cells in each layer,
- \mathbf{R} = positions of B1 sublattices in layer 1 which can be written as a linear combination, of the vectors \mathbf{a}_1 and \mathbf{a}_2 ,
- \mathbf{R}' = positions of A2 sublattices in layer 2 which can be written as a linear combination, of the vectors \mathbf{a}'_1 and \mathbf{a}'_2 ,

The vectors τ_α and τ'_β are not vanished when $\alpha = A$ and $\beta = B$, respectively. We can get the vectors \mathbf{a}'_1 and \mathbf{a}'_2 by rotating the vectors \mathbf{a}_1 and \mathbf{a}_2 , respectively. We change the notations of vectors \mathbf{a}_1 and \mathbf{a}_2 because it will make the reciprocal space look simpler. Fig.23 and 24 clarify the notion written above. The main difference between this model and the model of the first half is that the basis of this model are constructed differently, which can be seen from the fact that the normalized factor is not $1/\sqrt{N_{sc}}$ where N_{sc} is the number of supercell. Although \mathbf{p}, \mathbf{k} are not measured directly from the center of the first Brillouin zone of the supercell, they are related to the momentum states measured from the center of the first Brillouin zone of the supercell. The prime symbols denote the

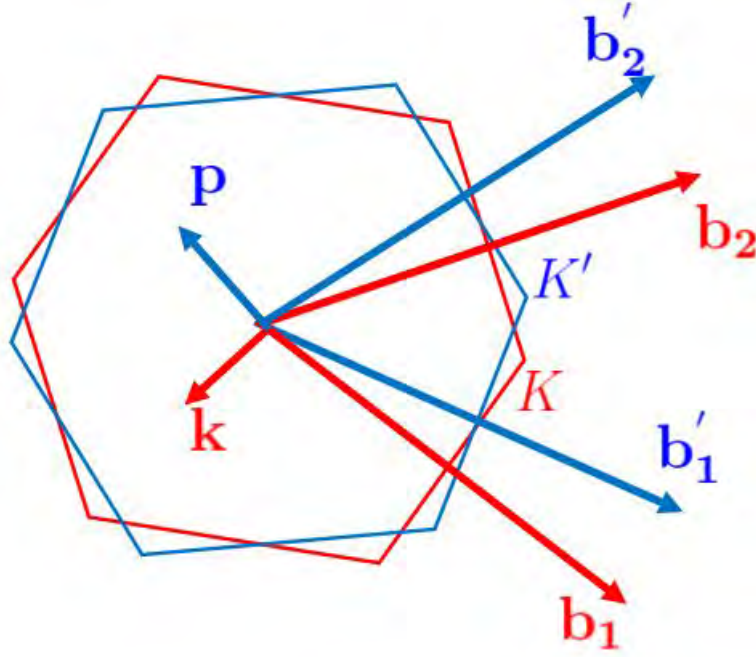


Figure 24: The notation of variables of the reciprocal space used in this model.

quantities related to the rotated layer. Next, We calculate tunneling amplitude between the momentum states in layer 1 and 2:

$$T_{\mathbf{k},\mathbf{p}}^{\alpha\beta} = \langle \psi_{\mathbf{k},\alpha}^1 | H | \psi_{\mathbf{p},\beta}^2 \rangle = \frac{1}{N_{uc}} \sum_{\mathbf{R}} \sum_{\mathbf{R}'} e^{-i\mathbf{k}(\mathbf{R}+\boldsymbol{\tau}_\alpha)+i\mathbf{p}(\mathbf{R}'+\boldsymbol{\tau}'_\beta)} \langle \mathbf{R} + \boldsymbol{\tau}_\alpha | H | \mathbf{R}' + \boldsymbol{\tau}'_\beta \rangle \quad (81)$$

$$= \frac{1}{N_{uc}} \sum_{\mathbf{R}} \sum_{\mathbf{R}'} e^{-i\mathbf{k}(\mathbf{R}+\boldsymbol{\tau}_\alpha)+i\mathbf{p}(\mathbf{R}'+\boldsymbol{\tau}'_\beta)} t(\mathbf{R} + \boldsymbol{\tau}_\alpha - \mathbf{R}' - \boldsymbol{\tau}'_\beta). \quad (82)$$

The form of the tunneling amplitude is the same as the one from Eq.77 but we will write it now as a function of a distance in the xy-plane r instead of the distance between carbon atoms or

$$t(\mathbf{r}) = A e^{-(\sqrt{r^2+h^2}-h)/\lambda} \frac{h^2}{r^2+h^2}. \quad (83)$$

The FT of the tunneling amplitude $t(\mathbf{r})$, which is a continuous on the real space function (MacDonald names this as a continuum model), between the localized wavefunction is

$$t(\mathbf{k}) = \int e^{-i\mathbf{k}\cdot\mathbf{r}} t(\mathbf{r}) d^2\mathbf{r} \quad (84)$$

$$= 2\pi \int_0^\infty r t(r) J_0(kr) dr. \quad (85)$$

The FT of the tunneling amplitude is simplified, written in a form of a Bessel function, because we are dealing with a circularly symmetric function here. Thus, the inverse FT of $t(\mathbf{k})$ is

$$t(\mathbf{r}) = \frac{1}{(2\pi)^2} \int e^{i\mathbf{k}\cdot\mathbf{r}} t(\mathbf{k}) d^2\mathbf{k} = \frac{1}{(2\pi)^2} \frac{(2\pi)^2}{A_{total}} \sum_{\mathbf{k}} e^{i\mathbf{k}\cdot\mathbf{r}} t(\mathbf{k}) = \frac{1}{A_{total}} \sum_{\mathbf{k}} e^{i\mathbf{k}\cdot\mathbf{r}} t(\mathbf{k}) \quad (86)$$

where $A_{total} = N_{uc}A_{uc}$ = the area of the each graphene sheet. Inserting the results from Eq.86 to 81 yields

$$T_{\mathbf{k},\mathbf{p}}^{\alpha\beta} = \frac{1}{N_{uc}} \sum_{\mathbf{R}} \sum_{\mathbf{R}'} e^{-i\mathbf{k}(\mathbf{R}+\boldsymbol{\tau}_\alpha)+i\mathbf{p}(\mathbf{R}'+\boldsymbol{\tau}'_\beta)} \left(\frac{1}{A_{total}} \sum_{\mathbf{k}'} e^{i\mathbf{k}'\cdot(\mathbf{R}+\boldsymbol{\tau}_\alpha-\mathbf{R}'-\boldsymbol{\tau}'_\beta)} t(\mathbf{k}') \right) \quad (87)$$

$$= \frac{1}{A_{uc}N_{uc}^2} \sum_{\mathbf{R}} \sum_{\mathbf{R}'} \sum_{\mathbf{k}'} e^{-i\mathbf{k}(\mathbf{R}+\boldsymbol{\tau}_\alpha)+i\mathbf{p}(\mathbf{R}'+\boldsymbol{\tau}'_\beta)} e^{i\mathbf{k}'\cdot(\mathbf{R}+\boldsymbol{\tau}_\alpha-\mathbf{R}'-\boldsymbol{\tau}'_\beta)} t(\mathbf{k}') \quad (88)$$

$$= \frac{1}{A_{uc}N_{uc}^2} \sum_{\mathbf{R}} \sum_{\mathbf{R}'} \sum_{\mathbf{k}'} e^{i(\mathbf{R}+\boldsymbol{\tau}_\alpha)(\mathbf{k}'-\mathbf{k})} e^{i(\mathbf{R}'+\boldsymbol{\tau}'_\beta)(\mathbf{p}-\mathbf{k}')} t(\mathbf{k}') \quad (89)$$

$$= \frac{1}{A_{uc}} \sum_{\mathbf{k}'} \left(\sum_{\mathbf{R}} \frac{e^{i\mathbf{R}(\mathbf{k}'-\mathbf{k})}}{N_{uc}} \right) \left(\sum_{\mathbf{R}'} \frac{e^{i\mathbf{R}'(\mathbf{p}-\mathbf{k}')}}{N_{uc}} \right) e^{i\boldsymbol{\tau}_\alpha(\mathbf{k}'-\mathbf{k})} e^{i\boldsymbol{\tau}'_\beta(\mathbf{p}-\mathbf{k}')} t(\mathbf{k}') \quad (90)$$

$$= \frac{1}{A_{uc}} \sum_{\mathbf{k}'} \left(\sum_{\mathbf{G}_1} \delta_{\mathbf{k}'-\mathbf{k},\mathbf{G}_1} \right) \left(\sum_{\mathbf{G}'_2} \delta_{\mathbf{p}-\mathbf{k}',-\mathbf{G}'_2} \right) e^{i\boldsymbol{\tau}_\alpha(\mathbf{k}'-\mathbf{k})} e^{i\boldsymbol{\tau}'_\beta(\mathbf{p}-\mathbf{k}')} t(\mathbf{k}') \quad (91)$$

$$= \frac{1}{A_{uc}} \sum_{\mathbf{G}_1} \sum_{\mathbf{G}'_2} \delta_{\mathbf{k}+\mathbf{G}_1,\mathbf{p}+\mathbf{G}'_2} e^{i\boldsymbol{\tau}_\alpha\mathbf{G}_1} e^{-i\boldsymbol{\tau}'_\beta\mathbf{G}'_2} t(\mathbf{k}') \quad (92)$$

$$= \frac{1}{A_{uc}} \sum_{\mathbf{G}_1} \delta_{\mathbf{k}+\mathbf{G}_1,\mathbf{p}+\mathbf{G}'_1} e^{i\boldsymbol{\tau}_\alpha\mathbf{G}_1} e^{-i(\boldsymbol{\tau}_\beta-\boldsymbol{\tau}_A)\mathbf{G}_1} t(\mathbf{k}+\mathbf{G}_1) \quad (93)$$

where

$$\mathbf{G}_1, \mathbf{G}'_2 = \text{linear combinations of reciprocal lattices vectors of the layer 1 and 2, respectively.} \quad (94)$$

We write $-\mathbf{G}'_2$ instead of \mathbf{G}'_2 in Eq.91, which is not change anything, so that there are only plus signs in the delta function in Eq.92. Because we want \mathbf{k} and \mathbf{p} to be as close as possible, which will be clarified later, the delta function in the Eq.92 is non-zero when \mathbf{G}_1 and \mathbf{G}'_2 are almost equal. This occur when there components are equal. Thus, after the summation over \mathbf{G}'_2 , only the terms where $\mathbf{G}'_2 = \mathbf{G}'_1$ (same components but difference basis) survive. We also write $(\boldsymbol{\tau}_\beta - \boldsymbol{\tau}_B)\mathbf{G}_1$ because the vectors $\boldsymbol{\tau}_\beta$ and \mathbf{G}'_2 are rotated with the same amount of angle which means the dot product between them will be the same if we write them in an unrotated form. Note that we write $\boldsymbol{\tau}_\beta - \boldsymbol{\tau}_B$ instead of $\boldsymbol{\tau}_\beta$ because the original notation of $\boldsymbol{\tau}'_\beta$ is the vector that points to a sub-lattice A in the rotated layer. Thus, if we want to write this vector in a form of vectors in the unrotated layer, we must them in the form shown above to keep its notation.

The form of the tunneling amplitude from Eq.93 may look different from the form on the MacDonald's paper because we have already summed on the vectors \mathbf{G}'_2 . A shorter form of the tunneling amplitude[8], which does not include the factor $e^{i\boldsymbol{\tau}_B\mathbf{G}_1}$,

$$T_{\mathbf{k},\mathbf{p}}^{\alpha\beta} = \frac{1}{A_{uc}} \sum_{\mathbf{G}_1} \delta_{\mathbf{k}+\mathbf{G}_1,\mathbf{p}+\mathbf{G}'_1} e^{i\boldsymbol{\tau}_\alpha\mathbf{G}_1} e^{-i\boldsymbol{\tau}_\beta\mathbf{G}_1} t(\mathbf{k}+\mathbf{G}_1) \quad (94)$$

can be obtained by using a new set of momentum states. For now, we will use the Eq.93 as the tunneling amplitude. However, both form of the tunnelling amplitudes will yield the same results as we can choose a basis that reduces the tunneling amplitude written in MacDonald's form to the form written here(he wrote how to do it in his paper).

2.2.3.1 Bilayer Graphene

In this section, we will use the result from Eq.94 to calculate the Hamiltonian of bilayer graphene. Then, we will compare the Hamiltonian obtained in this section with the one obtained from the method in the previous section. By using Eq.93, we can rewrite the tunneling matrix as

$$T_{\mathbf{k},\mathbf{p}}^{\alpha\beta} = \frac{1}{A_{uc}} \sum_{\mathbf{G}_1} \delta_{\mathbf{k}+\mathbf{G}_1,\mathbf{p}+\mathbf{G}_1} e^{i(\tau_\alpha-\tau_\beta+\tau_A)\mathbf{G}_1} t(\mathbf{k}+\mathbf{G}_1). \quad (95)$$

Note that $\mathbf{G}'_1 = \mathbf{G}_1$ for this case. From Eq.95, the delta function is not vanished when $\mathbf{k} = \mathbf{p}$. Thus, from

$$T_{\mathbf{k},\mathbf{k}}^{\alpha\beta} = \frac{1}{A_{uc}} \sum_{\mathbf{G}_1} e^{i(\tau_\alpha-\tau_\beta+\tau_A)\mathbf{G}_1} t(\mathbf{k}+\mathbf{G}_1). \quad (96)$$

Thus, from the tunneling matrix, we can construct a trial wavefunction as

$$|\Psi(\mathbf{k})\rangle = c_1 |A1, \mathbf{k}\rangle + c_2 |B1, \mathbf{k}\rangle + c_3 |A2, \mathbf{k}\rangle + c_4 |B2, \mathbf{k}\rangle. \quad (97)$$

And the resulting matrix has 4x4 dimension. Until now, we have not talked about the tunnelling amplitude within the same layer. However, this quantity can be easily calculated by using Eq.93 and setting \mathbf{G}_1 to equal to \mathbf{G}'_1 , which has already being done in this case, because we are considering the tunnelling in the same layer. We will have to replace $t(\mathbf{k})$ with $t_s(\mathbf{k})$ which is the FT of the tunneling amplitude within the same layer. The result is similar to the Eq.95 and we will write them as

$$T_{\mathbf{k}_1,\mathbf{k}_2}^{(s)\alpha\beta} = \frac{1}{A_{uc}} \sum_{\mathbf{G}_1} \delta_{\mathbf{k}_1,\mathbf{k}_2} e^{i(\tau_\alpha-\tau_\beta+\tau_A)\mathbf{G}_1} t_s(\mathbf{k}_1+\mathbf{G}_1) \sim \delta_{\mathbf{k}_1,\mathbf{k}_2} \quad (98)$$

where \mathbf{k}_1 and \mathbf{k}_2 are crystal momentum in the same reciprocal space. As you can see, the tunneling between momentum states within the same layer occur when their crystal momentums are equal. This result is general and we will use it later in the case of twisted bilayer graphene. Finally, the expression of the Hamiltonian in this case is

$$H_{BG} = \begin{bmatrix} \langle A1, \mathbf{k} | H | A1, \mathbf{k} \rangle & \langle A1, \mathbf{k} | H | B1, \mathbf{k} \rangle & \langle A1, \mathbf{k} | H | A2, \mathbf{k} \rangle & \langle A1, \mathbf{k} | H | B2, \mathbf{k} \rangle \\ \langle B1, \mathbf{k} | H | A1, \mathbf{k} \rangle & \langle B1, \mathbf{k} | H | B1, \mathbf{k} \rangle & \langle B1, \mathbf{k} | H | A2, \mathbf{k} \rangle & \langle B1, \mathbf{k} | H | B2, \mathbf{k} \rangle \\ \langle A2, \mathbf{k} | H | A1, \mathbf{k} \rangle & \langle A2, \mathbf{k} | H | B1, \mathbf{k} \rangle & \langle A2, \mathbf{k} | H | A2, \mathbf{k} \rangle & \langle A2, \mathbf{k} | H | B2, \mathbf{k} \rangle \\ \langle B2, \mathbf{k} | H | A1, \mathbf{k} \rangle & \langle B2, \mathbf{k} | H | B1, \mathbf{k} \rangle & \langle B2, \mathbf{k} | H | A2, \mathbf{k} \rangle & \langle B2, \mathbf{k} | H | B2, \mathbf{k} \rangle \end{bmatrix} \quad (99)$$

$$= \begin{bmatrix} 0 & -tf(\mathbf{k}) & T_{\mathbf{k},\mathbf{k}}^{AA} & T_{\mathbf{k},\mathbf{k}}^{AB} \\ -tf^*(\mathbf{k}) & 0 & T_{\mathbf{k},\mathbf{k}}^{BA} & T_{\mathbf{k},\mathbf{k}}^{BB} \\ \hline (T_{\mathbf{k},\mathbf{k}}^{AA})^* & (T_{\mathbf{k},\mathbf{k}}^{AB})^* & 0 & -tf(\mathbf{k}) \\ (T_{\mathbf{k},\mathbf{k}}^{BA})^* & (T_{\mathbf{k},\mathbf{k}}^{BB})^* & -tf^*(\mathbf{k}) & 0 \end{bmatrix}. \quad (100)$$

By using Eq.96 and

$$\boldsymbol{\tau}_A = -\frac{a}{\sqrt{3}}(1, 0), \quad \boldsymbol{\tau}_B = 0, \quad (101)$$

$$\mathbf{b}_1 = \frac{2\pi}{a} \left(\frac{1}{\sqrt{3}}, -1 \right), \quad \mathbf{b}_2 = \frac{2\pi}{a} \left(\frac{1}{\sqrt{3}}, 1 \right), \quad (102)$$

we can show that the tunneling amplitude between sub-lattices A1 and A2 is

$$T_{\mathbf{k},\mathbf{k}}^{AA} = \frac{1}{A_{uc}} \sum_{\mathbf{G}_1} e^{i\boldsymbol{\tau}_A \mathbf{G}_1} t(\mathbf{k} + \mathbf{G}_1). \quad (103)$$

If we look back to the section where we calculate this term, Eq.36, we can see that this term should be vanished and not depend on the crystal momentum \mathbf{k} . The reason for the vanishing of that term is because we approximate it. However, the tunneling amplitudes that we have derived here are more general which shows us that the real tunneling amplitudes between all sub-lattices will depend on the crystal momentum. In low energy regime, only the momentum states near the Dirac cone from each graphene sheet are interested. Thus, we will write

$$\mathbf{k} = \mathbf{K} + \mathbf{q} \quad (104)$$

where \mathbf{K} is the position of the Dirac cone in the reciprocal space of each graphene sheet and $|\mathbf{q}| \ll |\mathbf{K}|$ is a vector measured from the Dirac cone. Thus, we can approximate $T_{\mathbf{k},\mathbf{k}}^{AA}$ as

$$T_{\mathbf{k},\mathbf{k}}^{AA} \approx \frac{1}{A_{uc}} \left(t(\mathbf{K} + \mathbf{q}) + t(\mathbf{K} + \mathbf{q} + \mathbf{b}_1) e^{i\boldsymbol{\tau}_A \mathbf{b}_1} + t(\mathbf{K} + \mathbf{q} - \mathbf{b}_2) e^{-i\boldsymbol{\tau}_A \mathbf{b}_2} \right) \quad (105)$$

$$\approx \frac{1}{A_{uc}} \left(t(\mathbf{K}) + t(\mathbf{K} + \mathbf{b}_1) e^{i\boldsymbol{\tau}_A \mathbf{b}_1} + t(\mathbf{K} - \mathbf{b}_2) e^{-i\boldsymbol{\tau}_A \mathbf{b}_2} \right) \quad (106)$$

$$= \frac{t(\mathbf{K})}{A_{uc}} (1 + 2\cos(2\pi/3)) = 0. \quad (107)$$

We use only three terms because this three terms yield the same magnitude of the tunneling amplitude $t(\mathbf{K})$ while other terms give less magnitude than this. By repeating this procedures, we can also show that

$$T_{\mathbf{k},\mathbf{k}}^{BB} = T_{\mathbf{k},\mathbf{k}}^{AB} = 0 \quad \text{and} \quad T_{\mathbf{k},\mathbf{k}}^{BA} = 3 \frac{t(\mathbf{K})}{A_{uc}} = 0.34 \text{ eV}. \quad (108)$$

By using the Eq.84 to calculate the tunneling amplitude $t(\mathbf{K})$ and the area of an unit cell of graphene $A_{uc} = \sqrt{3}a^2/2 = 5.24 \text{ \AA}^2$, we can show that $T_{\mathbf{k},\mathbf{k}}^{BA} = 0.34 \text{ eV}$. Though, it is not equal to 0.39 eV, which is because it's an approximated value, the approximation using only three terms give a quite good result.

2.2.3.2 Twisted Bilayer Graphene

We will use Eq.93 to calculate the band structure of twisted bilayer graphene in this section. We can use the equation to calculate the band structure for each \mathbf{k} by constructing

the basis based on the values of \mathbf{k} , \mathbf{p} and \mathbf{G}_1 that yields non-zero delta function. We can see that there are many \mathbf{p} that yields non-zero delta function for each \mathbf{k} since $\mathbf{G}_1 \neq \mathbf{G}'_1$ but not when $\mathbf{G}_1 \approx \mathbf{G}'_1$. This means that the number of basis for a trial wavefunction in this case are quite large. For a general value of \mathbf{k} , it is hard to write a Hamiltonian for a system to because

- Numerically, the dimension of the Hamiltonian is very large which means we have to deal with a computationally expensive problem.
- Theoretically, we have to face with the convergence problem. In other words, it's not clear how many basis we should keep for each \mathbf{k} to determine the band structure analytically.

Both of this can be solve by choosing the value of \mathbf{k} that give most information to us. Because we know the the low energy states are situated near the Dirac points, this give us an intuitive idea that the momentum states near the Dirac points are account for the shape of the band structure(only for the low energy regime). For the momentum states near the Dirac point \mathbf{K} and \mathbf{K}' , we can write them as

$$\mathbf{k} = \mathbf{K} + \mathbf{q} \quad (109)$$

where

$$\mathbf{K} = \text{The Dirac point of the unrotated layer 1,} \quad (110)$$

$$\mathbf{q} = \text{The momentum vector measured with respect to the Dirac point } \mathbf{K} \quad (111)$$

and

$$\mathbf{p} = \mathbf{K}' + \mathbf{q}' \quad (112)$$

where

$$\mathbf{K}' = \text{The Dirac point of the rotated layer 2,} \quad (113)$$

$$\mathbf{q}' = \text{The momentum vector measured with respect to the Dirac point. } \mathbf{K}' \quad (114)$$

Fig.25 shows the vectors \mathbf{q} and \mathbf{q}' . We will now clarify why the components of the reciprocal lattice vectors in the kronecker delta must be equal if we only interested in the low energy regime. From Eq.92, the kronecker delta can be satisfied when

$$\mathbf{K} + \mathbf{q} + \mathbf{G}_1 = \mathbf{K}' + \mathbf{q}' + \mathbf{G}'_2. \quad (115)$$

If $\mathbf{G}_1 = \mathbf{b}_2$ and $\mathbf{G}'_2 = 0$ and $|\mathbf{q}| \ll |\mathbf{K}|$, see Fig.26, we can see that the kronecker can be satisfied when the magnitude of \mathbf{q} is large. This will contradict the assumption of the vectors \mathbf{q} . If the components of the reciprocal lattice vectors are equal, which are all zeros in this case, see Fig.27, we can see that the kronecker can be satisfied while the magnitude of \mathbf{q} and \mathbf{q}' satisfied the assumption. This is the reason why we set the components of the reciprocal lattice vectors from each layer to be equal. Now, we can rewrite the tunneling matrix, from Eq.93, as

$$T_{\mathbf{K}+\mathbf{q}, \mathbf{K}'+\mathbf{q}'}^{\alpha\beta} = \frac{1}{A_{uc}} \sum_{\mathbf{G}_1} \delta_{\mathbf{q}-\mathbf{q}', \mathbf{K}'-\mathbf{K}+\mathbf{G}'_1-\mathbf{G}_1} e^{i(\tau_\alpha - \tau_\beta + \tau_A)\mathbf{G}_1 \cdot \mathbf{t}} t(\mathbf{k} + \mathbf{G}_1). \quad (116)$$

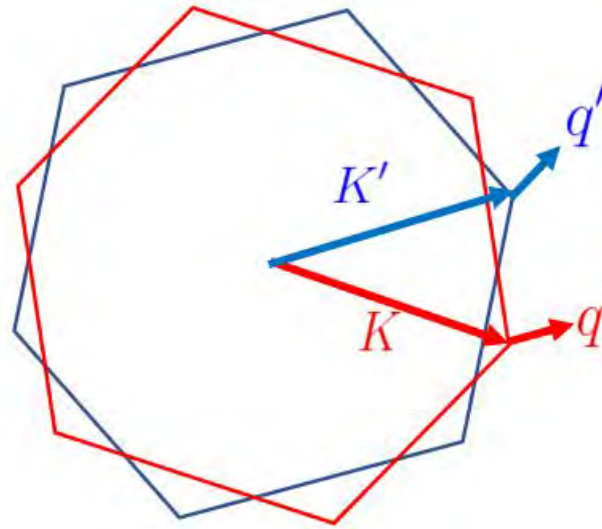


Figure 25: q and q' are measured with respect to the Dirac cones of each layer.

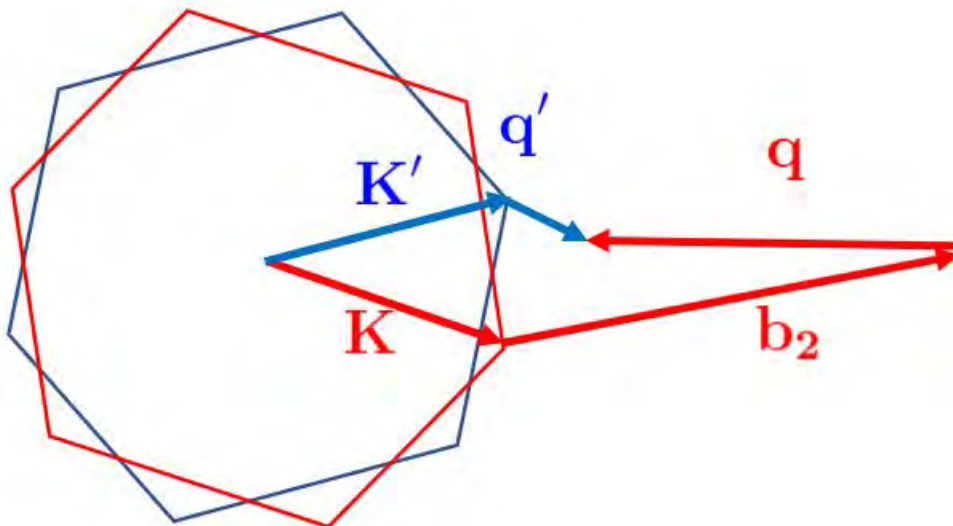


Figure 26: If the components of reciprocal lattice vectors from both layers are not equal, the magnitude of q (or q' in other cases) will be too large.

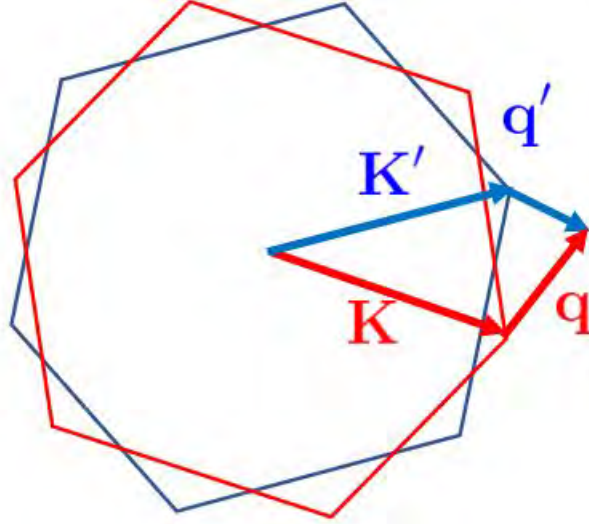


Figure 27: If the components of reciprocal lattice vectors are equal, the kronecker can be satisfied while the magnitudes of \mathbf{q} and \mathbf{q}' are still much less than $|\mathbf{K}|$.

For each twist angle, the quantity $\mathbf{K}' - \mathbf{K}$ which is the shift of Dirac point between two layers are constant which we will write as

$$\mathbf{K}' - \mathbf{K} = \mathbf{q}_D. \quad (117)$$

Because \mathbf{G}_1 and \mathbf{G}'_1 have the same components(different basis),

$$\mathbf{G}'_1 - \mathbf{G}_1 = n(\mathbf{b}'_1 - \mathbf{b}_1) + m(\mathbf{b}'_2 - \mathbf{b}_2), \quad (118)$$

$$= n\mathbf{b}_1^m + m\mathbf{b}_2^m. \quad (119)$$

The definition of vectors \mathbf{b}_1^m and \mathbf{b}_2^m is shown in Fig.28. Eq.116 can be rewritten now as

$$T_{\mathbf{K}+\mathbf{q},\mathbf{K}'+\mathbf{q}'}^{\alpha\beta} = \frac{1}{A_{uc}} \sum_{n,m} \delta_{\mathbf{q}-\mathbf{q}',\mathbf{q}_D+n\mathbf{b}_1^m+m\mathbf{b}_2^m} e^{i(\tau_\alpha-\tau_\beta+\tau_A)\mathbf{G}_{1(n,m)}\cdot\mathbf{t}} t(\mathbf{K}+\mathbf{q}+\mathbf{G}_{1(n,m)}). \quad (120)$$

From Eq.116, we can see that the tunneling amplitude is not vanished when

$$\mathbf{q} - \mathbf{q}' = \mathbf{q}_D + n\mathbf{b}_1^m + m\mathbf{b}_2^m \quad (121)$$

or when the differences between \mathbf{q} and \mathbf{q}' are equal to $\mathbf{q}_D + n\mathbf{b}_1^m + m\mathbf{b}_2^m$. Let's approximate $\mathbf{q} = 0$ in the argument of function t as $|\mathbf{q}| \ll |\mathbf{K}|$, we can see that, from Fig.24,

$$t(\mathbf{K}) = t(\mathbf{K} - \mathbf{b}_1) = t(\mathbf{K} - \mathbf{b}_2) \quad (122)$$

because they are the same Dirac cone. Thus, for a momentum state $|\mathbf{q}\rangle$, which should be written as $|\mathbf{q} + \mathbf{K}\rangle$ but we omit \mathbf{K} , where \mathbf{q} is near the Dirac point, we can use Eq.116 to write the tunneling matrix as

$$T_{\mathbf{K}+\mathbf{q},\mathbf{K}'+\mathbf{q}'}^{\alpha\beta} \approx \frac{t(\mathbf{K})}{A_{uc}} \delta_{\mathbf{q}-\mathbf{q}',\mathbf{q}_D} + \frac{t(\mathbf{K})}{A_{uc}} e^{i(\tau_\alpha-\tau_\beta+\tau_A)\mathbf{b}_1\cdot\mathbf{t}} \delta_{\mathbf{q}-\mathbf{q}',\mathbf{q}_D-\mathbf{b}_1^m} + \frac{t(\mathbf{K})}{A_{uc}} e^{-i(\tau_\alpha-\tau_\beta+\tau_A)\mathbf{b}_2\cdot\mathbf{t}} \delta_{\mathbf{q}-\mathbf{q}',\mathbf{q}_D-\mathbf{b}_2^m}. \quad (123)$$

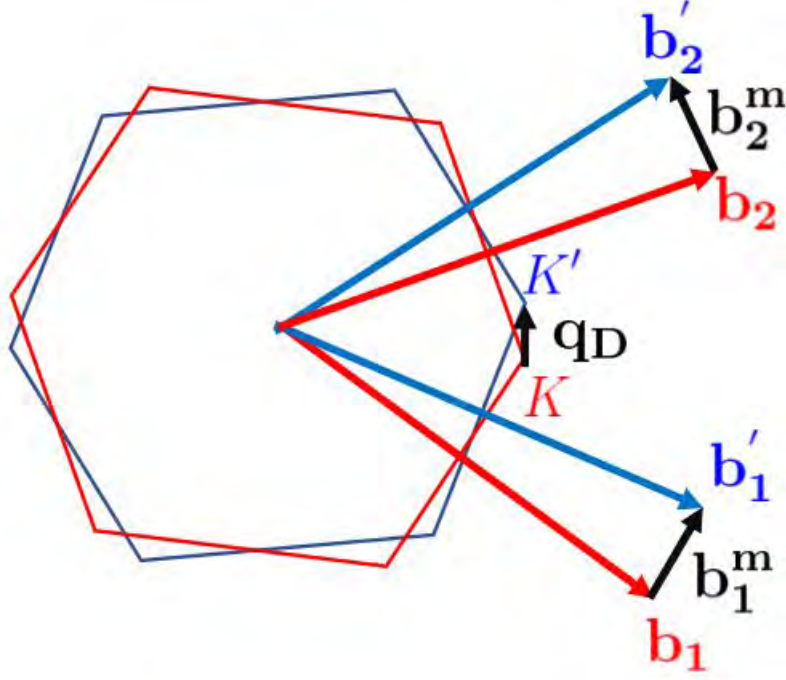


Figure 28: b_1^m and b_2^m

We can also write the Eq.123 as the form of a matrix as

$$T_{\mathbf{K}+\mathbf{q},\mathbf{K}'+\mathbf{q}'} = \begin{bmatrix} T^{AA} & T^{AB} \\ T^{BA} & T^{BB} \end{bmatrix}_{\mathbf{K}+\mathbf{q},\mathbf{K}'+\mathbf{q}'} \quad (124)$$

$$\approx \frac{t(\mathbf{K})}{A_{uc}} \begin{bmatrix} 1 & 1 \\ 1 & 1 \end{bmatrix} \delta_{\mathbf{q}-\mathbf{q}',\mathbf{q}_D} + \frac{t(\mathbf{K})}{A_{uc}} \begin{bmatrix} 1 & 1 \\ 1 & 1 \end{bmatrix} \delta_{\mathbf{q}-\mathbf{q}',\mathbf{q}_D+\mathbf{b}_1^m} + \frac{t(\mathbf{K})}{A_{uc}} \begin{bmatrix} 1 & 1 \\ 1 & 1 \end{bmatrix} \delta_{\mathbf{q}-\mathbf{q}',\mathbf{q}_D-\mathbf{b}_2^m} \quad (125)$$

$$= T_1 \delta_{\mathbf{q}-\mathbf{q}',\mathbf{q}_D} + T_2 \delta_{\mathbf{q}-\mathbf{q}',\mathbf{q}_D-\mathbf{b}_1^m} + T_3 \delta_{\mathbf{q}-\mathbf{q}',\mathbf{q}_D-\mathbf{b}_2^m} \quad (126)$$

We will also write a momentum state from the rotated layer as $|\mathbf{q}'\rangle$ instead of writing $|\mathbf{q}' + \mathbf{K}'\rangle$. The (minimal) number of basis for the Hamiltonian for \mathbf{q} near the Dirac point \mathbf{K} are 8;

$$|\mathbf{q}', A(B)2\rangle, |\mathbf{q} + \mathbf{q}_D, A(B), 1\rangle, |\mathbf{q}' + \mathbf{q}_D - \mathbf{b}_1^m, A(B), 2\rangle, |\mathbf{q}' + \mathbf{q}_D - \mathbf{b}_2^m, A(B), 2\rangle. \quad (127)$$

The tunneling matrix between the momentum states in the rotated layer $|\mathbf{q}', A2\rangle, |\mathbf{q}', B2\rangle$ can be calculated by using the result from the Eq.17. From the equation, we can see that we can write the tunneling matrix between the momentum states of the unrotated layer as

$$H_{low,\mathbf{K}}^{eff}(\mathbf{q}) = -\frac{\sqrt{3}ta}{2} \begin{bmatrix} 0 & q_x - q_y i \\ q_x + q_y i & 0 \end{bmatrix} = -\frac{\sqrt{3}ta}{2} |\mathbf{q}| \begin{bmatrix} 0 & e^{i\theta_q} \\ e^{i\theta_q} & 0 \end{bmatrix} \quad (128)$$

where $\tan(\theta) = q_y/q_x$. As you can see, θ_q is measured with respect to x-axis. This means that we can obtain the tunneling matrix between the momentum states of the

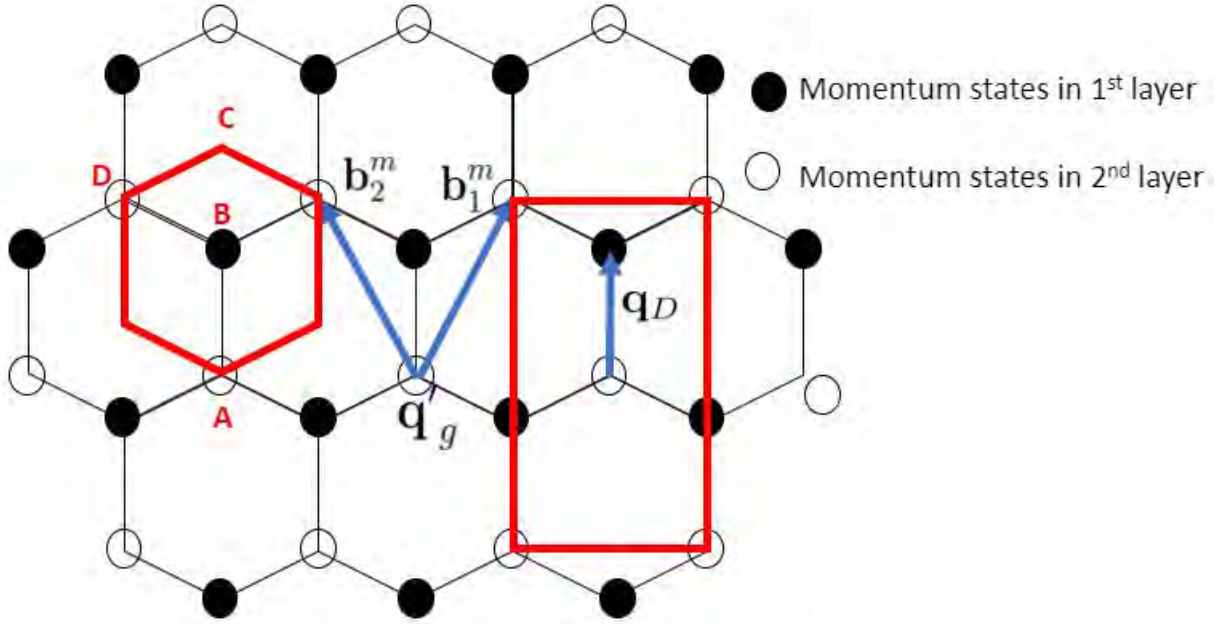


Figure 29: The reciprocal space spanned by reciprocal lattice vectors \mathbf{b}_1^m and \mathbf{b}_2^m . The high symmetry lines are drawn along the points A, B, C, D and A. The rectangle denotes the area of the first Brillouin zone.

rotated layer by rotating the x-axis. Thus, the tunneling matrix between the momentum states of the rotated layer can be easily obtained from the Eq.105 by changing $\theta_{q'}$, which is measured with respect to the x-axis, to $\theta_{q'} - \theta$ where θ is the twist angle which gives

$$H_{low,K'}^{eff}(\mathbf{q}') = -\frac{\sqrt{3}ta}{2} |\mathbf{q}'| \begin{bmatrix} 0 & e^{i(\theta_{q'} - \theta)} \\ e^{i(\theta_{q'} - \theta)} & 0 \end{bmatrix}. \quad (129)$$

Now, we can constructing the Hamiltonian by using the momentum states from the Eq.4 as

$$H_{low}(\mathbf{q}) = \begin{bmatrix} H_{low,K}^{eff}(\mathbf{q}') & T_1 & T_2 & T_3 \\ T_1^\dagger & H_{low,K'}^{eff}(\mathbf{q} - \mathbf{q}_D) & 0 & 0 \\ T_2^\dagger & 0 & H_{low,K'}^{eff}(\mathbf{q}' + \mathbf{q}_D - \mathbf{b}_1^m) & 0 \\ T_3^\dagger & 0 & 0 & H_{low,K'}^{eff}(\mathbf{q}' + \mathbf{q}_D - \mathbf{b}_2^m) \end{bmatrix} \quad (130)$$

In general, we can construct a trial wavefunction from the momentum states as

$$|\psi(\mathbf{q})\rangle = \sum_{n,m} c_{\mathbf{q}}^{n,m} |\mathbf{q}' + \mathbf{q}_D + n\mathbf{b}_1^m + m\mathbf{b}_2^m\rangle + \sum_{n',m'} c_{\mathbf{q}-\mathbf{q}_D}^{n',m'} |\mathbf{q}' + n'\mathbf{b}_1^m + m'\mathbf{b}_2^m\rangle. \quad (131)$$

From Eq.127, replacing \mathbf{q} with $\mathbf{q} + n\mathbf{b}_1^m + m\mathbf{b}_2^m$ does not change the form of the Hamiltonian. This means the reciprocal lattice vectors of This momentum space are

$$\mathbf{b}_1^m \quad \text{and} \quad \mathbf{b}_2^m. \quad (132)$$

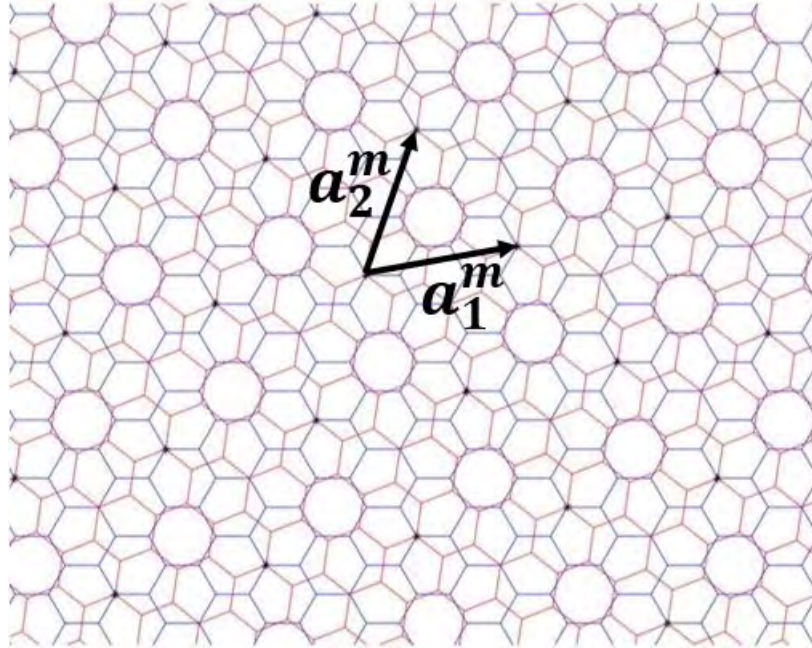


Figure 30: This figure shows a superlattice of twisted bilayer graphene with a twist angle equal to 21.79° . The black dots denote places where carbon atoms are dense. In this case, carbon atoms superimpose at each black dot. Moiré structure formed by the black dots are spanned by the vectors \mathbf{a}_1^m and \mathbf{a}_2^m .

Fig.29 shows a repeated zone scheme of the momentum space of the wave function of electrons described by Eq131. We can use \mathbf{b}_1^m and \mathbf{b}_2^m to calculate the lattice vectors for Moiré pattern shown in Fig.30.

Chapter 3

Methodology

I will list a few steps required for calculating the band structure of twisted bilayer graphene for large and small twist angles.

3.1 Large twist angles

1. determine the coordinates of sub-lattices in a supercell for each twist angle determined by m and r . This can be done by choosing a set of coordinates of electrons near the origin and write them in the basis of the superlattice vectors. For example, if $\mathbf{r}_{n,m} = n\mathbf{a}_1 + m\mathbf{a}_2$ is a coordinate of an electron, we can write it as

$$\mathbf{r}_{n,m} = n\mathbf{a}_1 + m\mathbf{a}_2 \rightarrow \mathbf{r}_{n,m} = n'\mathbf{R}_1 + m'\mathbf{R}_2. \quad (133)$$

Next, we will choose only n' and m' that are less than 1 as these are the coordinates of electrons in the supercell marked by superlattice vectors \mathbf{R}_1 and \mathbf{R}_2 .

2. use Eq.76 to determine the tunneling amplitude between sub-lattices which are components of the Hamiltonian.

3.2 Small twist angles

1. select momentum states from both layer, see Appendix A.
2. use Eq.120 to calculate the tunneling amplitude between momentum states. It's better to calculate the tunneling amplitudes between both layers first as they are not depend on the crystal momentum \mathbf{q} .

Chapter 4

Result

4.1 Band structure along high symmetry lines and Bandwidth

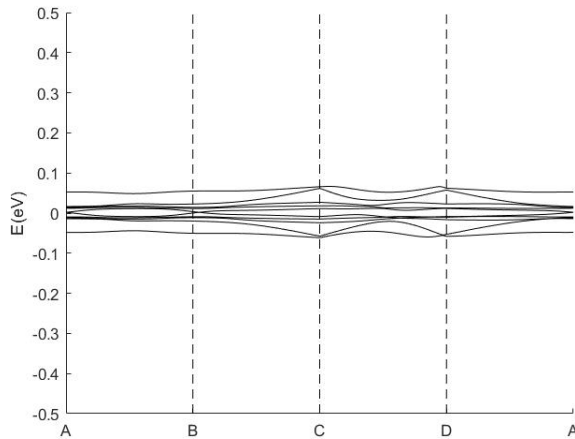


Figure 31: 0.5 degree

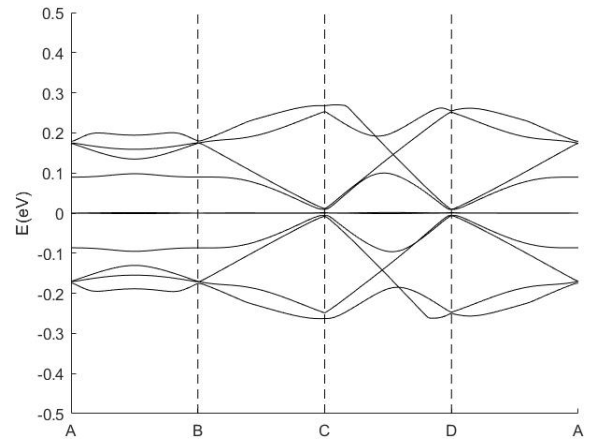


Figure 32: 1.05 degree

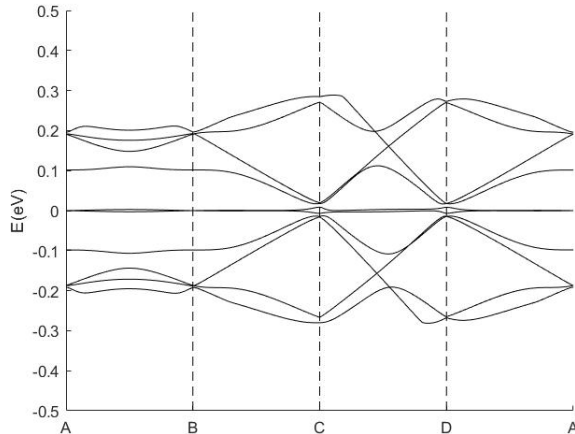


Figure 33: 1.08 degree

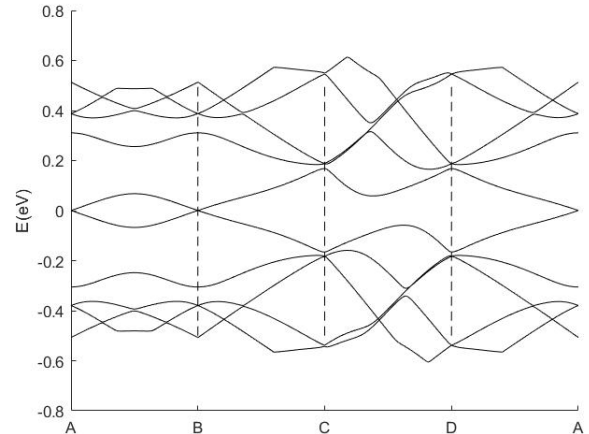


Figure 34: 2.00 degree

In this section, we will show you the band structures along high symmetry lines of 4 twist angles. The reason that we only focus on low twist angle is the low energy model only valid in this region. As you can see from Fig.31-34, the differences between the highest energy of the conduction band and the lowest energy of the valence, called Bandwidth, can be easily seen from these figures but not in Fig.32. The conduction band and valence bands shown in Fig.32 are almost straight lines in this energy scale, eV. We can see from these figures that the Bandwidth is not always increased when the twist angle is increased. For example, increasing the twist angle from 0.5 degree

to 1.05 degree tends to decrease the Bandwidth while increasing the twist angle from 1.05 degree to 1.08 degree tends to increase the Bandwidth. Fig.35-38 show the

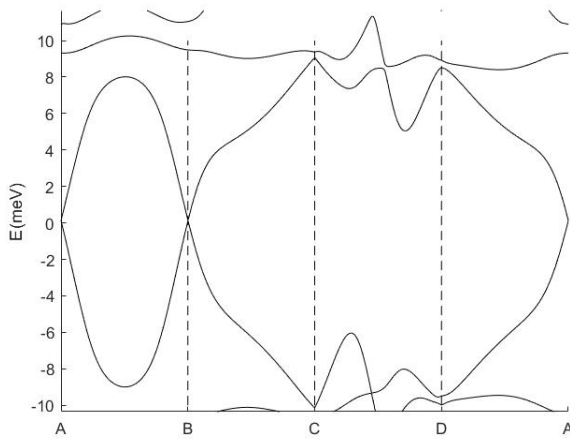


Figure 35: 0.5 degree

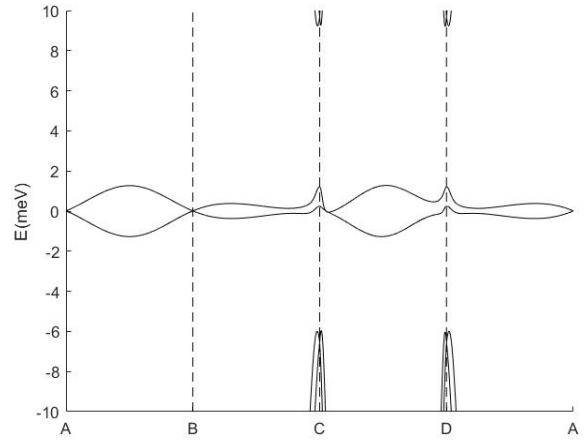


Figure 36: 1.05 degree

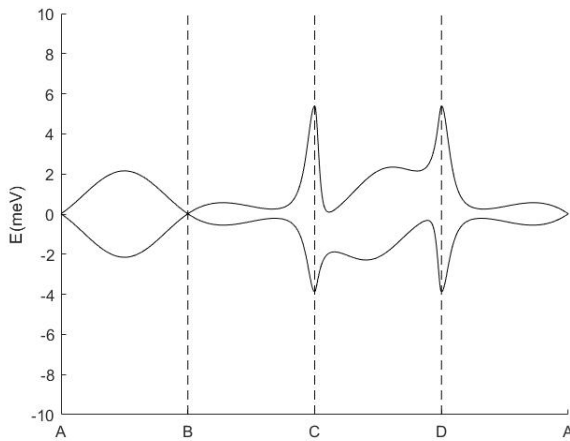


Figure 37: 1.08 degree

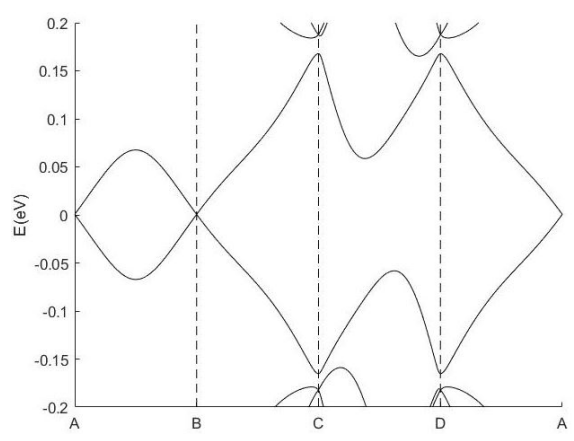


Figure 38: 2.00 degree

conduction bands and valence bands of 4 twist angles in the energy scales that we can see their bandwidths clearly. The band structures shown in Fig.35-37 are plotted in the energy scale meV while Fig.38 shows the band structure in the energy scale eV. We can see that the twist angle at 1.05 degree yields smallest bandwidth. There are also energy gaps which sandwich the conduction and valence bands shown in Fig.36. Fig.39 shows the bandwidth for all twist angles from 0 degree to 1.5 degree calculated by using the energies plotted along high symmetry lines. there is a local minimum at 1.05 degree. For the very low twist angles, less than 0.1 degree, we can see that the bandwidths are even less than the bandwidth at 1.05 degree. At 0 degree, the bandwidth is vanished completely! This is because the moire pattern is disappear at very low twist angles, $b_{1(2)}^m \rightarrow 0$, this means we can't get plot the band structures along high symmetry lines anymore. But we know that the band structure of twisted

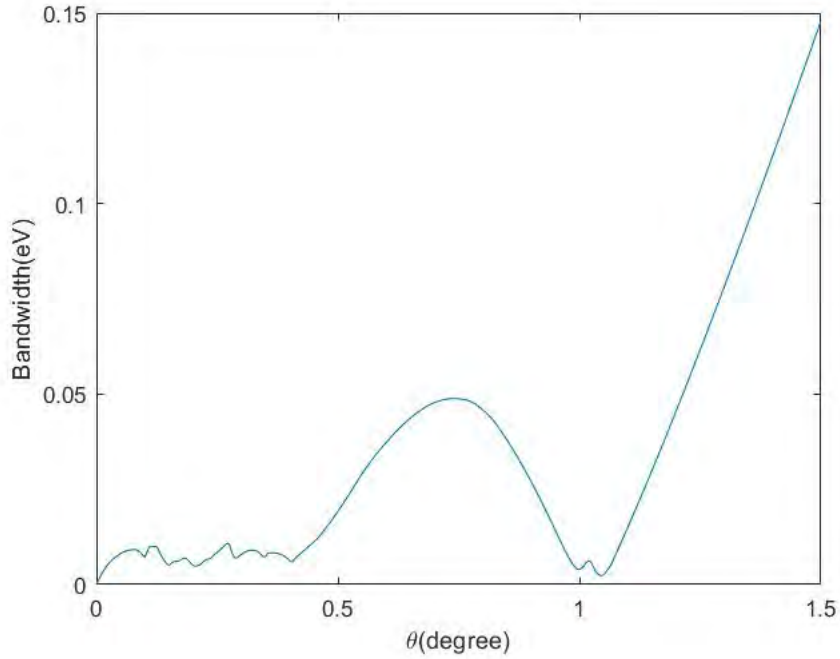


Figure 39: The bandwidth of Moire pattern. Each value is calculated from the difference between the maximum of the conduction band and the minimum of the valence band for each twist angle.

bilayer graphene when there is no twist angle is equal to the band structure of bilayer graphene. Because the bandwidth of bilayer graphene, see Fig.13, is higher than the bandwidth of twisted bilayer graphene at 1.05 degree. We conclude that the twist angle at 1.05 degree yields smallest bandwidth.

4.2 three-dimensional band structures and Fermi surface

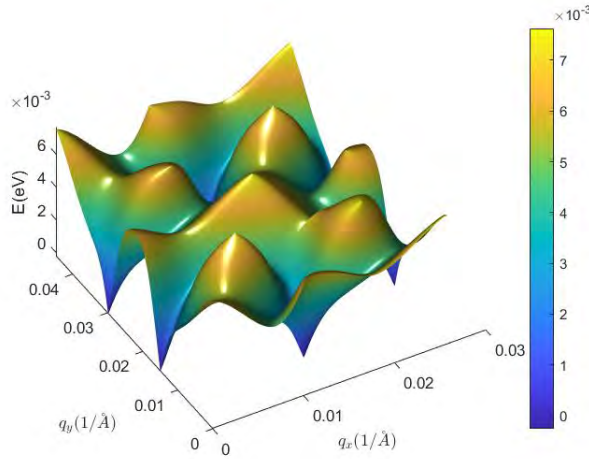


Figure 40: 0.5 degree

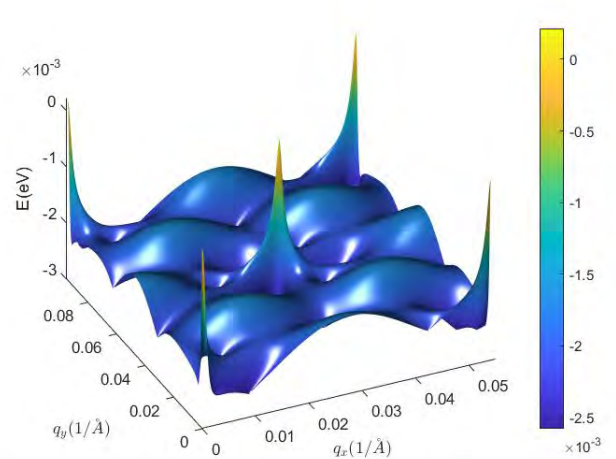


Figure 41: 1.05 degree

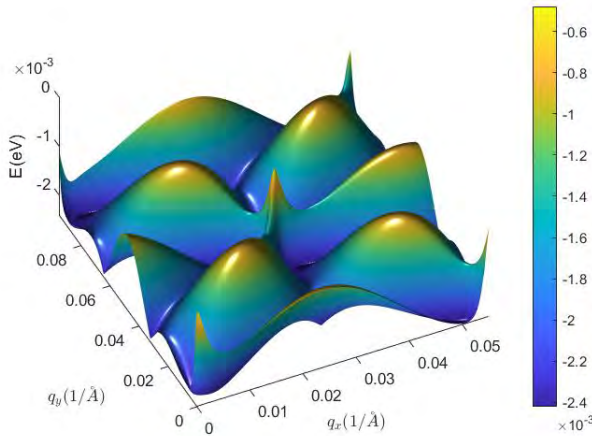


Figure 42: 1.08 degree

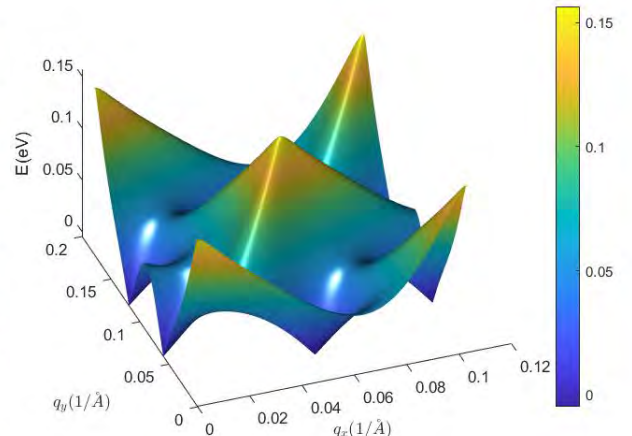


Figure 43: 2.00 degree

In this section, we plot three-dimensional band structures of 4 twist angles in the region specified by the rectangle shown in Fig.29. The colors shown in these figures specify the energy levels of electrons. If the proportions of the yellow and blue regions are almost equal, the energies of electrons are largely distributed. Thus, we can clearly see from Fig.40-43 that the energies of electrons in the energy band with twist angle equal to 1.05 degree distribute less than other twist angles. Fig.44 shows the Fermi surface of twist bilayer graphene calculated from Fig.41. We can see that the momentum states of electrons that have high energies situated near the center of the figure are less than the momentum states of electrons that have low energies colored as blue.

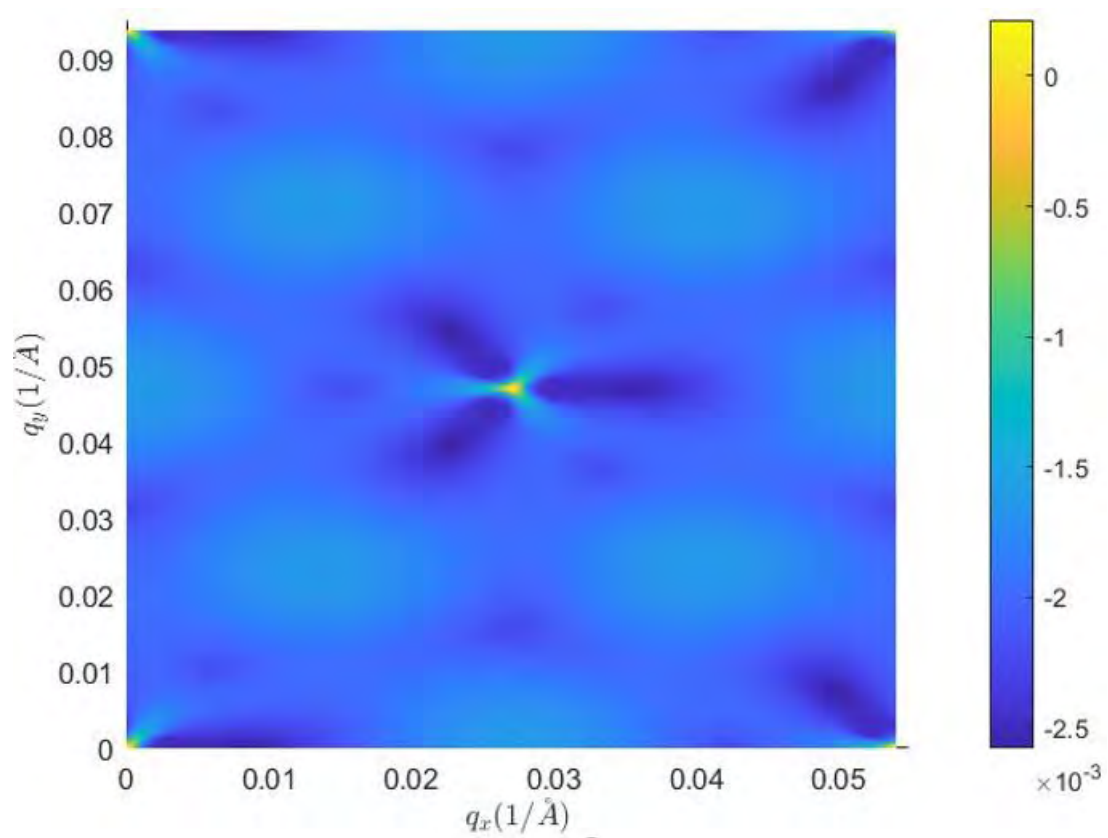


Figure 44: The Fermi surface of the conduction band when the twist angle is equal to 1.05 degree.

4.3 Density of states

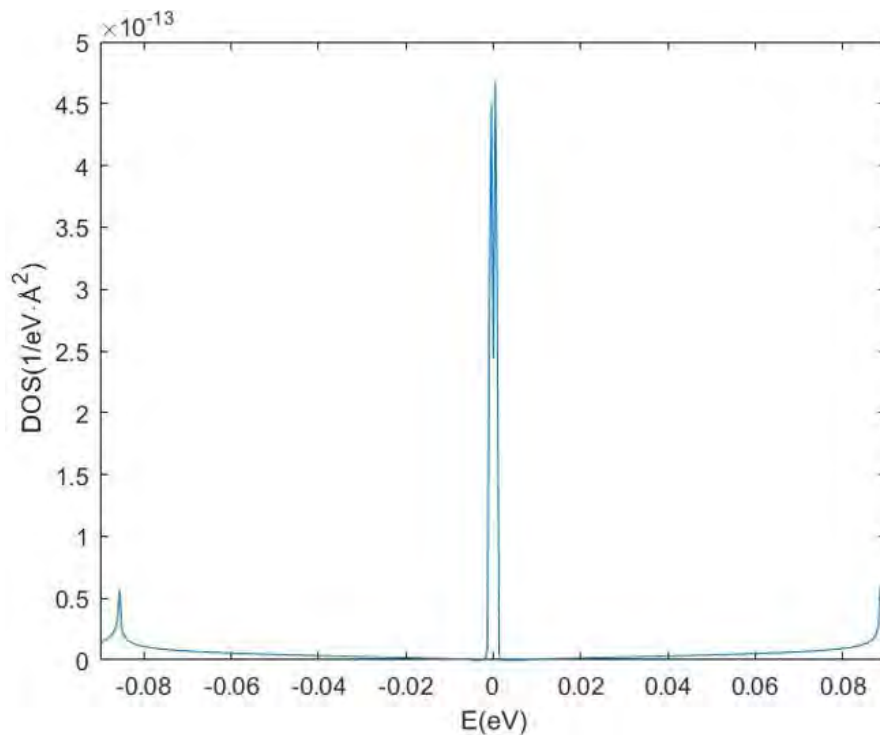


Figure 45: The density of states of twisted bilayer graphene with the twist angle equal to 1.05 degree.

The density of states of twisted bilayer graphene with twist angle equal to 1.05 degree is shown in Fig.45. As you can see, the density of states near the Fermi energy is very high compared to other regions. Because there are energy gaps on both sides of the Fermi energy, the density of states on both sides of the Fermi energy are zero. Fig.46 shows the density of states for each energy level. Having high density of states near the Fermi energy means there is a chance for us to change carrier density to that energy level. If the temperature of our twisted bilayer graphene is very low and the carrier density is at the level where the density of states is high, there is a chance that the twisted bilayer graphene to be a superconductor. This is because the kinetic energies of electrons are small over the wide range which means the potential energies from the Coulomb potential will dominate. This strong interaction which occurs at this energy level can leads to the superconducting state in twisted bilayer graphene. If we change the carrier density to the region where the density of states is vanished. There is a chance that we could get an insulator. The reason why we call 1.05 degree the magic angle is there are many states that twisted bilayer graphene can be when the twist angle is equal to 1.05.

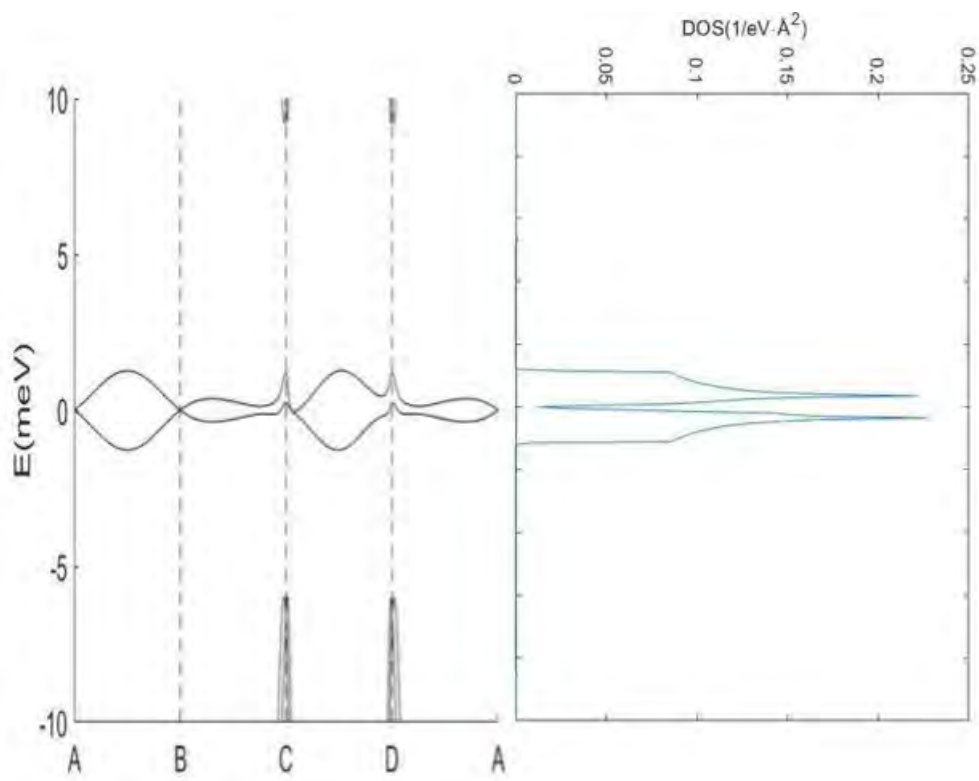


Figure 46: The conduction and valence bands of twisted bilayer graphene with twist angle equal to 1.05 degree and the density of states.

Chapter 5

Conclusion

In conclusion, we have written the codes for determining the band structures of graphene, bilayer graphene and twisted bilayer graphene. For twisted bilayer graphene, we have written two separated codes for calculating the band structures for large twist angles and low twist angles. We also write codes to calculate the density of states of the untwisted(twisted) bilayer graphene. The density of states of graphene and bilayer graphene obtained from our model have similar shapes to other literatures. In case of twisted bilayer graphene, we obtain the energy gaps on both sides of the Fermi energy which is agree with the minimal model proposed by X. Lin[8]. The magic angle, or the angle that yields smallest bandwidth, obtained from our model is precisely equal to 1.05 degree which is agree with the continuum model proposed by MacDonald[6].

Appendix

```
1 param_band = genvar_band(4,1.05);
2 qx = 0;
3 qy = 0;
4 E_b_tBLG(qx,qy,151,param_band);
```

In this section, We will show the Matlab code that we use to calculate the band structure, density of states, Fermi surface of twisted bilayer graphene according to MacDonald's model. The code above shows how can we calculate energies for a crystal momentum (q_x, q_y) . First, 1 generates the necessary parameters using the function `genvar_band(B, angle)` where `B` and `angle`(degree) are the quantity relating to the number of basis, which we will clarify later, and the twist angle. We found that the energy bands are converged when $C \geq 3$. We stored the parameters in the variable `param_band` in case we want to modify it later. Next, 2 and 3 specify the crystal momentum that we want to calculate the energies. Last, 4 calculate the energies specified by the parameters from the previous lines using the function `E_b_tBLG(qx, qy, N, param_band)` where the variable `N` specifies the band that we want to obtain the energy. If there are `M` bands, we can get the energy of the valence and conduction bands by using $N = M/2-1$ and $N = M/2+1$, respectively. Appendixes A and B below show the code of the functions used in the code above. The Fermi surface can be easily calculated by using the function `contour`. Appendix C show how can we use the functions from Appendixes A and B to calculate the denisty of states.

Appendix A

We will show how the function `genvar_band` works in this section.

```
1 function f = genvar_band(B, angle)
2 t = B;
3 %extract coordinate
4 %%%%%%%%%%%
5 if t == 0
6     C = [[0,0];[0,1];[-1,0]];
7 elseif t ==1
8     C = [[0,0];[0,1];[-1,0];[1,0];[1,1];[1,2];...
9         [0,2];[-1,1];[-2,0];[-2,-1];[-1,-1];[0,-1]];
10 else
11     C = [[0,0];[0,1];[-1,0];[1,0];[1,1];[1,2];...
12         [0,2];[-1,1];[-2,0];[-2,-1];[-1,-1];[0,-1]];
13     for i = 2:t
14         p1 = [0+i,0];
15         p2 = [0,0-i];
16         p3 = [-1-i,0-i];
17         p4 = [-1-i,0];
18         p5 = [0,1+i];
19         p6 = [0+i,1+i];
20     C = [C;p1];
```

```

21     C = [C;p2];
22     C = [C;p3];
23     C = [C;p4];
24     C = [C;p5];
25     C = [C;p6];
26     %line1
27     for j = 1:i-1
28         C = [C;p1+j*[-1,-1]];
29     end
30     %line2
31     for j = 1:i
32         C = [C;p2+j*[-1,0]];
33     end
34     %line3
35     for j = 1:i-1
36         C = [C;p3+j*[0,1]];
37     end
38     %line4
39     for j = 1:i
40         C = [C;p4+j*[1,1]];
41     end
42     %line5
43     for j = 1:i-1
44         C = [C;p5+j*[1,0]];
45     end
46     %line6
47     for j = 1:i
48         C = [C;p6+j*[0,-1]];
49     end
50 end
51 end
52 %%%%%%%%%%%
53 V0 = 0.39;
54 lambda = 0.27;
55 d0 = 3.35; % distance between layer
56 d = 1.42;
57 dhex = sqrt(3)*d;
58 a1 = [1/2;sqrt(3)/2]*dhex;
59 a2 = [-1/2;sqrt(3)/2]*dhex;
60 b1 = [sqrt(3)/2;1/2]*4*pi/(3*d);
61 b2 = [-sqrt(3)/2;1/2]*4*pi/(3*d);
62 Rt = @(ang) [cos(ang),-sin(ang);sin(ang),cos(ang)];
63 K = [4*pi/(3*dhex);0];
64 Auc = sqrt(3)*dhex^2/2; % Area of an unit cell
65 theta = (angle)*pi/180;
66 hbarvf = 6.582; % eV*Angstrom

```

```

67
68 %Kt point(rotated K point → theta/2) and rotated vectors
69 Kt1 = Rt(theta/2)*K; %K point of above layer
70 Kt2 = Rt(-theta/2)*K;%K point of lower layer
71 b1t = Rt(theta/2)*b1; % above layer
72 b2t = Rt(theta/2)*b2; % above layer
73 b3t = Rt(-theta/2)*b1;% lower layer
74 b4t = Rt(-theta/2)*b2;% lower layer
75 Kt1 = Kt1';
76 Kt2 = Kt2';
77 b1t = b1t';
78 b2t = b2t';
79 b3t = b3t';
80 b4t = b4t';
81 bm1 = b3t-b1t;
82 bm2 = b4t-b2t;
83 qb = Kt2-Kt1;
84 expo1 = exp(1i*(theta/2));
85 expo2 = exp(1i*(-theta/2));
86
87 H0 = zeros(4*size(C,1),4*size(C,1));
88 H1 = zeros(4*size(C,1),4*size(C,1));
89 for i = 1:2*size(C,1) % the rest can be calculated by putting
    the hermitian conjugate on them
90     % i == row , j = column
91     u = 1;
92     col = 0;
93     for j = 2*size(C,1)+1:4*size(C,1)
94         diff1 = C(floor((j-2*size(C,1)+1)/2),1)-C(floor((i+1)
95             /2),1);
96         diff2 = C(floor((j-2*size(C,1)+1)/2),2)-C(floor((i+1)
97             /2),2);
98         kvec = norm(Kt1+diff1*b1t+diff2*b2t);
99         G1 = diff1*b1t+diff2*b2t;
100        G2 = G1;
101        fun = @(x) 2*pi.*V0.*x.*exp(-(sqrt(x.*x+d0^2)-d0)./
102            lambda).*...
103            (1./(x.*x+d0^2)).*d0^2.*besselj(0,kvec.*x);
104        if mod(i,2) == 1 % this mean i → sub A
105            tau1 = [0,0];
106        else
107            tau1 = Rt(theta/2)*[0;1]*d;
108            tau1 = tau1';
109        end
110        if mod(j,2) == 1 % this mean j → sub A
111            tau2 = [0,0];

```

```

109         else
110             tau2 = Rt(theta/2)*[0;1]*d;
111             tau2 = tau2';
112         end
113         H0(i,j) = (integral(fun,0,inf)/Auc)*exp(1i*(dot(G1,tau1
114             )-dot(G2,tau2)));
115         H0(j,i) = H0(i,j)';
116         col = col+1;
117         if col == 2
118             u = u+1;
119             col = 0;
120         end
121     end
122
123     f{1} = C;
124     f{2} = bm1;
125     f{3} = bm2;
126     f{4} = hbarvf;
127     f{5} = expo1;
128     f{6} = expo2;
129     f{7} = qb;
130     f{8} = H1;
131     f{9} = H0;
132     f{10} = Kt1;
133     f{11} = Kt2;
134 end

```

The lines 2-51 create basis according to the value of B . The number of basis can be easily understood from Fig.47. The lines 53-57 specify the tunneling parameters[8]. From Eq.130, we can see that the low-energy Hamiltonian of tBLG can be separated to the non-diagonal and diagonal parts, H_0 and H_1 , respectively. The lines 89-121 create the non-diagonal part H_0 . We calculate this part in this code because this part is not depend the crystal momentum. Doing this will help us the reduce the time used for calculating the whole energy bands. The lines 123-131 send all calculated variables to the indices.

Appendix B

In this section, we will use the parameters and variables generated from the function `genvar_band` to calculate the energy bands.

```

1 function e = E_b_tBLG(qx, qy, s, f)
2
3     f{1} = C;
4     f{2} = bm1;
5     f{3} = bm2;
6     f{4} = hbarvf;
7     f{5} = expo1;

```

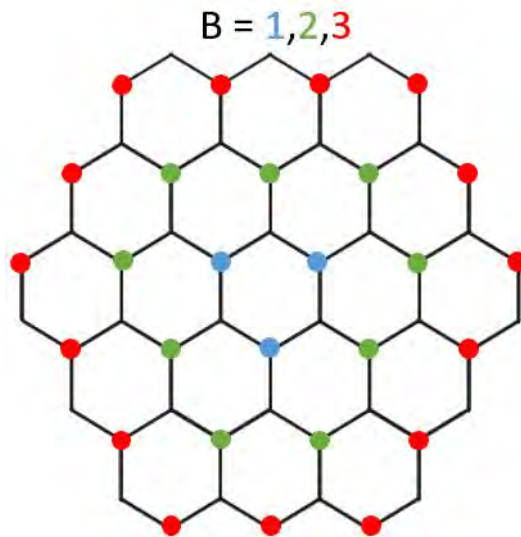


Figure 47: When you specify $B = 1$, the number of K-points used in the calculation. In this case, the total number of basis should be $(3+1)*2$ according to Eq.130 where the number 1 is added to account for the tunneling within the unrotated layer and the number 2 accounts for the sub-lattices A and B. However, we want the basis in each layer to be equal which means we will use the same number of K-points from each layer. Thus, the number of basis used in our program is equal to $(3+3)*2$.

```

8     f{6} = expo2;
9     f{7} = qb;
10    f{8} = H1;
11    f{9} = H0;
12    f{10} = Kt1;
13    f{11} = Kt2;
14
15    t = 3.03;
16
17    ux = mod(qx, sqrt(3)*norm(qb));
18    uy = mod(qy, 3*norm(qb));
19    %define matrix
20    u = 1;
21    col = 0;
22    for v = 1:2:2*size(C,1)-1
23        qx2 = ux+C(u,1)*bm1(1)+C(u,2)*bm2(1);
24        qy2 = uy+C(u,1)*bm1(2)+C(u,2)*bm2(2);
25        k1 = Kt1'+[qx2;qy2];
26        u1 = exp(1i*dot(k1,d1))+exp(1i*dot(k1,d2))+exp(1i*
                dot(k1,d3));
27        H1(v:v+1,v:v+1) = -t*[0,u1;u1',0];
28        col = col+1;
29        if col == 1
30            u = u+1;
31            col = 0;
32    end

```

```

33     end
34     u = 1;
35     col = 0;
36     for v = 2*size(C,1)+1:2:4*size(C,1)-1
37         qx2 = ux+qb(1)+C(u,1)*bm1(1)+C(u,2)*bm2(1);
38         qy2 = uy+qb(2)+C(u,1)*bm1(2)+C(u,2)*bm2(2);
39         k2 = Kt2'+[qx2;qy2];
40         u2 = exp(1i*dot(k2,dt1))+exp(1i*dot(k2,dt2))+exp(1i
            *dot(k2,dt3));
41         H1(v:v+1,v:v+1) = -t*[0,u2;u2',0];
42         col = col+1;
43         if col == 1
44             u =u+1;
45             col = 0;
46         end
47     end
48     E(1,:) = eig(H1+H0);
49     e = E(1,s);
50 end

```

The lines 2-13 retrieve the parameters and variables from the function `param_band`. the line 13 specifies the tunneling amplitude between carbon-carbon atoms. The lines 17, 18 are included to solve the problem of non-periodic band structures when the ranges of the crystal momentums q_x and q_y are too large. This occurs because 1) we only keep only the finite number of basis 2) we use the low-energy Hamiltonians of graphene in the diagonal part of H_1 which are not periodic, see Eq.18. Because we use $C \geq 3$, there is no discontinuity in the boundaries, marked by the rectangle in Fig.29, of the momentum space which means it's correct to include the lines 17 and 18. Fig.48,49 show the differences in the boundary of the momentum space. You can see that the difference is almost vanished when $C = 3$. Next, the lines 20-50 calculate the components for the diagonal Hamiltonian H_1 .

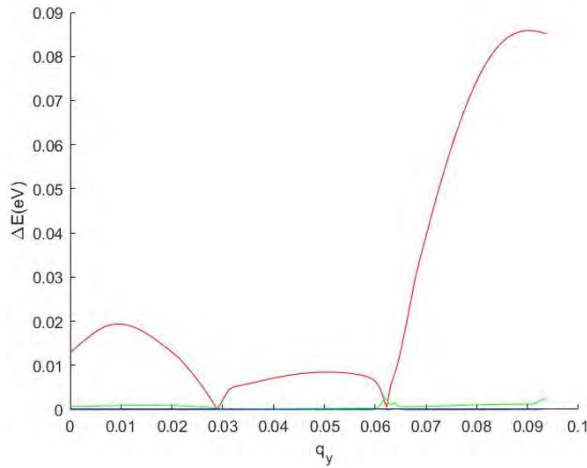


Figure 48: The three lines show the differences in the energies where $q_y = 0$ and $q_y = 3|q_b|$ which are the boundaries of the momentum space. The red, green and blue show the difference in the energies when $C = 2, 3$ and 4 , respectively. As you can see, the order of ΔE for the red line is in the order 10^{-2} eV which is quite large. Thus, it's invalid to use the function `E_b_tBLG` in this case.

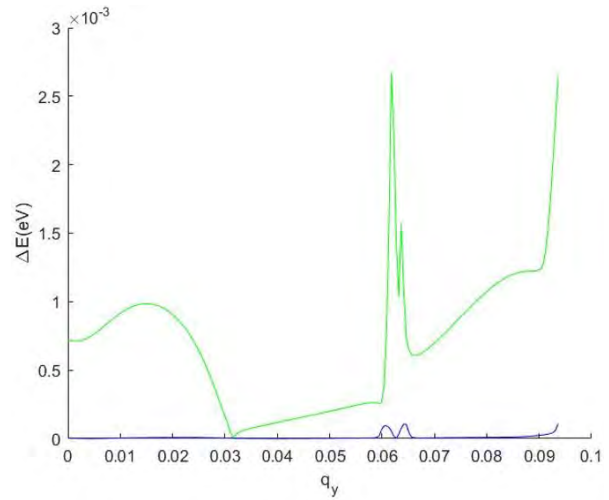


Figure 49: The values of ΔE decrease substantially when we increase C . The order of ΔE when $C=3$ is 10^{-3} while it's equal to 10^{-4} when $C=4$. Thus, we the function `E_b_tBLG` is valid when $C \geq 3$.

Appendix C

This part use the result from the appendixes A and B to calculate the density of states of twisted bilayer graphene. The area of the first Brillouin zone is shown in Fig.29.

```

1 param_band = genvar_band(4,1.05);
2 qb = param_band{7};
3 Nx = 400;
4 Ny = 400;
5
6 minx = 0;
7 maxx = sqrt(3)*norm(qb);
8 miny = 0;
9 maxy = 3*norm(qb);
10
11 dx = (maxx-minx)/Nx;
12 dy = (maxy-miny)/Ny;
13 E = zeros(Ny+1,Nx+1,4*size(C,1));
14 expo1 = exp(1i*(theta/2));
15 expo2 = exp(1i*(-theta/2));
16 for nkx = 1:Nx+1
17     qx = minx+dx*(nkx-1);
18     for nky = 1:Ny+1
19         qy = miny+dy*(nky-1);
20         for b = 1:4*size(C,1)
21             E(nky,nkx,b) = ...

```

```

22         E_b_tBLG(qx, qy, 2* size(C, 1), param_band);
23     end
24 end
25 end
26
27 min_e = -0.09;
28 max_e = 0.09;
29 Ne = 400;
30 dez = (max_e-min_e)/Ne;
31 dA = dx*dy;
32 cof = dA/(2*pi*pi*dez);
33 DOSX = min_e:dez:max_e;
34 DOSY = zeros(1, size(DOSX, 2));
35
36 for ne = 1:Ne+1
37     count = 0;
38     ez = min_e+dez*(ne-1);
39     for layer_energy = 2*size(C, 1)-5:2*size(C, 1)+5
40         tms1 = E(:, :, layer_energy);
41         for i = 1:Nx+1
42             tms2 = tms1(i, :);
43             for j = 1:Ny+1
44                 if abs(ez-tms2(j)) < 0.5*dez
45                     count = count+1;
46                 end
47             end
48         end
49     end
50     DOSY(ne) = count;
51 end
52 DOSY = cof*DOSY;

```

The lines 1-4 generate parameters and the number of grids used for calculating the density of states. The lines 6-9 specify the boundaries of the Brillouin zone, see Fig.29. The lines 11-19 calculate the energy bands within the Brillouin zone. The lines 27 and 30 denote the range of energy we want to calculate the density of states where N_e is the number of discretized energy. The lines 31 and 32 give the coefficient shown in Eq.27. The lines 36-51 count the number of states within each energy range.

References

- [1] P. R. Wallace, “The band theory of graphite,” *Phys. Rev.*, vol. 71, pp. 622–634, May 1947.
- [2] K. S. Novoselov, “Electric field effect in atomically thin carbon films,” *Science*, vol. 306, p. 666–669, Oct 2004.
- [3] E. McCann, “Electronic properties of monolayer and bilayer graphene,” *NanoScience and Technology*, p. 237–275, 2011.
- [4] P. E. Allain and J. N. Fuchs, “Klein tunneling in graphene: optics with massless electrons,” *The European Physical Journal B*, vol. 83, p. 301–317, Oct 2011.
- [5] M. I. Katsnelson, K. S. Novoselov, and A. K. Geim, “Chiral tunnelling and the klein paradox in graphene,” *Nature Physics*, vol. 2, no. 9, pp. 620–625, 2006.
- [6] R. Bistritzer and A. H. MacDonald, “Moiré bands in twisted double-layer graphene,” *Proceedings of the National Academy of Sciences*, vol. 108, no. 30, pp. 12233–12237, 2011.
- [7] Y. Cao, V. Fatemi, S. Fang, K. Watanabe, T. Taniguchi, E. Kaxiras, and P. Jarillo-Herrero, “Unconventional superconductivity in magic-angle graphene superlattices,” *Nature*, vol. 556, pp. 43 EP –, Mar 2018. Article.
- [8] X. Lin and D. Tománek, “Minimum model for the electronic structure of twisted bilayer graphene and related structures,” *Physical Review B*, vol. 98, Aug 2018.
- [9] A. O. Sboychakov, A. L. Rakhmanov, A. V. Rozhkov, and F. Nori, “Electronic spectrum of twisted bilayer graphene,” *Phys. Rev. B*, vol. 92, p. 075402, Aug 2015.
- [10] Y. Zhang, Y.-W. Tan, H. L. Stormer, and P. Kim, “Experimental observation of the quantum hall effect and berry’s phase in graphene,” *Nature*, vol. 438, pp. 201–204, Nov 2005.
- [11] Z. Jiang, Y. Zhang, Y.-W. Tan, H. Stormer, and P. Kim, “Quantum hall effect in graphene,” *Solid State Communications*, vol. 143, no. 1, pp. 14 – 19, 2007. Exploring graphene.
- [12] K. S. Novoselov, Z. Jiang, Y. Zhang, S. V. Morozov, H. L. Stormer, U. Zeitler, J. C. Maan, G. S. Boebinger, P. Kim, and A. K. Geim, “Room-temperature quantum hall effect in graphene,” *Science*, vol. 315, no. 5817, pp. 1379–1379, 2007.